Spring 2022

Review of Current Reactive Force Field Potentials for Use in Simulating the Atomic Layer Deposition of Alumina on Aluminum

Devon T. Romine
Missouri State University, devonromine14@gmail.com

REVIEW OF CURRENT REACTIVE FORCE FIELD POTENTIALS FOR USE IN

SIMULATING THE ATOMIC LAYER DEPOSITION OF ALUMINA ON ALUMINUM

A Master's Thesis

Presented to

The Graduate College of

Missouri State University

In Partial Fulfillment

Of the Requirements for the Degree

Master of Science, Materials Science

By

Devon Romine

May 2022

REVIEW OF CURRENT REACTIVE FORCE FIELD POTENTIALS FOR USE IN SIMULATING THE ATOMIC LAYER DEPOSITION OF ALUMINA ON ALUMINUM

Physics, Astronomy, and Materials Science

Missouri State University, May 2022

Master of Science

Devon Romine

ABSTRACT

Alumina has recently garnered quite a bit of attention for use as a tunnel barrier in Josephson tunnel junctions. The quality of the metal oxide layer in the Josephson tunnel junction is a key factor in its effectiveness. To optimize the deposition method of alumina, we need a deep understanding of the large-scale surface interactions that cannot be reached using ab initio molecular dynamics. In this study, I have compared two existing reactive force field (ReaxFF) parameters to determine their abilities to model the atomic layer deposition (ALD) of alumina on an aluminum surface. ReaxFF molecular dynamics was chosen because it is capable of modeling larger systems for longer time periods than the ab initio molecular dynamics. I have reviewed the capabilities of the parameters to model stable precursors and reactions paths for the surface reactions of the ALD process utilizing LAMMPS and Amsterdam Modeling Suites (AMS) software. A comparison of the relaxed positions of the precursors and optimized energies of the reaction steps are used to determine the deficiencies of current parameters, allowing for a more focused reparameterization in future studies.

KEYWORDS: reactive force field, molecular dynamics, alumina, atomic layer deposition, modeling

REVIEW OF CURRENT REACTIVE FORCE FIELD POTENTIALS FOR USE IN

SIMULATING THE ATOMIC LAYER DEPOSITION OF ALUMINA ON ALUMINUM

By

Devon Romine

A Master's Thesis
Submitted to the Graduate College
Of Missouri State University
In Partial Fulfillment of the Requirements
For the Degree of Master of Science, Materials Science

May 2022

Approved:

Ridwan Sakidja, Ph.D., Thesis Committee Chair

Robert Mayanovic, Ph.D., Committee Member

David Cornelison, Ph.D., Committee Member

Julie Masterson, Ph.D., Dean of the Graduate College

In the interest of academic freedom and the principle of free speech, approval of this thesis indicates the format is acceptable and meets the academic criteria for the discipline as determined by the faculty that constitute the thesis committee. The content and views expressed in this thesis are those of the student-scholar and are not endorsed by Missouri State University, its Graduate College, or its employees.

ACKNOWLEDGEMENTS

I would also like to thank the following people for their support during the course of my graduate studies: Dr. Ridwan Sakidja for your constant guidance and for showing me the way to becoming a better researcher, Dr. David Cornelison and Dr. Robert Mayanovic for your support and patience through some of the more difficult times in my life, and especially my wife, Kathryn. You have been by my side throughout my academic career. Without you pushing me to be the person you saw in me all those years ago, I would never have made it this far.

I dedicate this thesis to George Cooper. You always told me I would make it this far and pushed me to believe in myself. You were a great man in life that always saw the best in people.

TABLE OF CONTENTS

LIST OF TABLES

LIST OF FIGURES

INTRODUCTION

Motivation

Josephson junctions are often used in microelectronics including superconducting qubits [1], which are topics of high interest in the advancement of quantum computing. Josephson tunnel junctions are formed from a superconducting metal-insulator-superconducting metal interface. A prevailing issue in the development of tunnel junctions for quantum usage is the existence of two-level systems (TLS) at the interface of the amorphous insulator (typically a metal oxide) and the metal [2]. The presence of these decoherent TLS in large numbers causes low and high-frequency noise in electronic systems that, due to the incredibly sensitive nature of superconducting qubits, makes it difficult to build an efficient quantum device.[3]. Many theories as to the source of these TLS in amorphous metal oxides exist and many of them have one commonality, defects at the metal oxide metal interface allow for stronger coupling and lead to varying potential barrier heights. [2]

Al-AlO$_x$-Al interfaces are commonly used as Josephson junctions due to the large band gap of alumina. [4-7] Thus a method of depositing alumina (Al$_2$O$_3$) that is defect free is required to make high-efficiency quantum devices. Computational studies into the deposition of alumina using DFT and molecular dynamics (MD) have been done [1, 4, 5, 8], but no comprehensive study of the existing reactive force fields for the application of atomic layer deposition (ALD) on aluminum has been done. In this study I attempt this review as a way of determining how well the existing force fields can describe the ALD process, and where they need to be improved.

The Atomic Layer Deposition Process

Atomic layer deposition (ALD) is a type of chemical vapor deposition (CVD) in which two or more vapor phase precursors are systematically pulsed onto the target substrate. The key element of ALD is that the surface interactions in each precursor pulse are self-limiting. [9, 10] This means that the vapor bonds to open sites on the surface until saturation is reached, after which no interactions will take place regardless of the number of vapor molecules left available. The self-limiting nature of the deposition means that after the adsorption limit in a region of the substrate has been reached, subsequent reactions must occur in another region leading to a uniform and defect free deposition.

ALD of alumina utilizing the precursors tri-methyl-aluminum (TMA) and vapor phase H2O has been an industry standard since the 1990's and has continued to be used since. [9, 11-15] The entire deposition process can be described as $2Al(CH3)3 + 3H_2O \rightarrow Al_2O_3 + 3CH_4$ can be broken into 4 partial reaction pathways that represent the surface interactions during the TMA and H2O pulse phases.

1) |-OH + AlM$_3$ (g) → |-O-AlM$_2$ + CH$_4$(g)

2) |-O-AlM$_2$ + H$_2$O(g) → |-O-AlM-OH +CH$_4$(g)

3) |-O-AlM-OH + H$_2$O(g) → |-O-Al(OH)$_2$ + CH$_4$(g)

4) |-O-Al(OH)$_2$ + AlM$_3$(g) → |-O-Al(OH)-O-AlM$_2$ + CH$_4$(g)
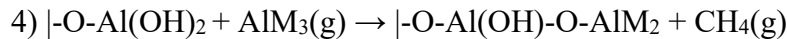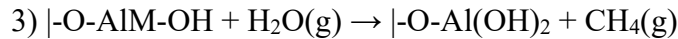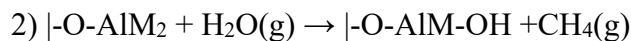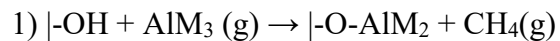
Where | denotes the aluminum surface and M denotes the methyl (CH$_3$) units. The first equation represents the TMA pulse interacting with the hydroxylated surface through the mechanism of ligand exchanges between TMA and the hydrogen of the surface hydroxyl units. The methyl

units then form methane (CH$_4$) and dissociate from the surface. The TMA pulse is self-terminating due to the steric nature of the methyl groups and will deposit until there are no more open areas to contain the methyl groups. Reactions 2 and 3 are gas phase water interacting with methyl aluminum surface. They form ligand exchanges with all the remaining methyl groups on the surface forming methane gas, then they dissociate onto the oxygen bridges, forming a bilayer of alumina and aluminum hydroxide [9, 10]. Experimental studies have shown the optimal temperature of the deposition to be between 150-200°C [8] and the optimal oxygen pressure under 25 Pa. [7]

Reactive Force Fields

Overview. Reactive force fields (ReaxFF) use classical approximations of quantum mechanical calculations. Like most force fields the total energy of the system is calculated using partial energies as seen in the equation

$$E_{total} = E_{bond} + E_{lp} + E_{over} + E_{under} + E_{val} + E_{pen} + E_{coa} + E_{triple} + E_{tors} + E_{conj} +$$
$$E_{H-bond} + E_{vdWaals} + E_{Coulomb} \text{ [16]}.$$

In a reactive system the bonding of respective atoms is varied based on how coordinated the atom is. Fully coordinated atoms will have interactions that decay quickly, known as short-range interactions, while undercoordinated atoms will have a much longer range of interactions due to their delocalized valence electrons. [17] The modeling of these more abstract concepts requires the use of a bond order term that can be used to calculate not only the bond energies due to 2, 3, and 4 body interactions, but energy penalties due to lone pair interactions, over coordination, and under coordination as well. I will not go into detail about all of these components, but I find it is important to describe some of the more prevalent aspects of the force field.

Bond Order. The bond orders are assumed to be obtained directly from the distance between atoms (r_{ij}) as seen in the equation

$$BO_{ij} = e^{\rho_{bo,1}(\frac{r_{ij}}{r_0})^{\rho_{bo,2}}} + e^{\rho_{bo,3}(\frac{r_{ij}^\pi}{r_0})^{\rho_{bo,4}}} + e^{\rho_{bo,5}(\frac{r_{ij}^{\pi\pi}}{r_0})^{\rho_{bo,6}}}$$

. Here we see that the bond order is dependent on three exponential terms. The sigma bond BO_{ij}^σ ($\rho_{bo,1}$, $\rho_{bo,2}$), the pi bond BO_{ij}^π ($\rho_{bo,3}$, $\rho_{bo,4}$), and the double pi bond $BO_{ij}^{\pi\pi}$ ($\rho_{bo,5}$, $\rho_{bo,6}$). The bond order is corrected for any over coordination and any 1-3 valence bond orders using the following equations

$$BO_{ij,corr}^\sigma = BO_{ij}^\sigma \cdot f_1(\Delta_i', \Delta_j') \cdot f_4(\Delta_i', BO_{ij}) \cdot f_5(\Delta_j', BO_{ij})$$

$$BO_{ij,corr}^\pi = BO_{ij}^\pi \cdot f_1(\Delta_i', \Delta_j') \cdot f_1(\Delta_i', \Delta_j') \cdot f_4(\Delta_i', BO_{ij}) \cdot f_5(\Delta_j', BO_{ij})$$

$$BO_{ij,corr}^{\pi\pi} = BO_{ij}^{\pi\pi} \cdot f_1(\Delta_i', \Delta_j') \cdot f_1(\Delta_i', \Delta_j') \cdot f_4(\Delta_i', BO_{ij}) \cdot f_5(\Delta_j', BO_{ij})$$

$$BO_{ij,corr} = BO_{ij,corr}^\sigma + BO_{ij,corr}^\pi + BO_{ij,corr}^{\pi\pi}$$

$$f_1((\Delta_i', \Delta_j') = \frac{1}{2}\left(\frac{Val_i + f_2(\Delta_i', \Delta_j')}{Val_i + f_2(\Delta_i', \Delta_j') + f_3(\Delta_i', \Delta_j')} + \frac{Val_j + f_2(\Delta_i', \Delta_j')}{Val_j + f_2(\Delta_i', \Delta_j') + f_3(\Delta_i', \Delta_j')}\right)$$

$$f_2(\Delta_i', \Delta_j') = e^{-\lambda_1\Delta_i'} + e^{-\lambda_1\Delta_j'}$$

$$f_3(\Delta_i', \Delta_j') = \frac{1}{\lambda_2}\ln\left(\frac{1}{2} \cdot (e^{-\lambda_2 \cdot \Delta_i'} + e^{-\lambda_2 \cdot \Delta_j'})\right)$$

$$f_4(\Delta_i', BO_{ij}) = \frac{1}{1 + e^{-\lambda_3 \cdot (\lambda_4 \cdot BO_{ij} \cdot BO_{ij} - \Delta_i') + \lambda_5}}$$

$$f_5(\Delta_j', BO_{ij}) = \frac{1}{1 + e^{-\lambda_3 \cdot (\lambda_4 \cdot BO_{ij} \cdot BO_{ij} - \Delta_j') + \lambda_5}}$$

$$\Delta_i' = \sum_{j=1}^{nbonds} BO_{ij} - Val_i$$

Val_i is the valency of the atom, Δ_i' is the over coordination of the atom and is defined as the difference between the bond order and the valency, and λ_x. are trained parameters.

Bond Energy. The corrected bond order, denoted BO_{ij} from now, are then used to calculate the bond energy $E_{bond} = -D_e^{\sigma} \cdot BO_{ij}^{\sigma} \cdot e^{\lambda_6(1-(BO_{ij}^{\sigma})^{\lambda_7})} - D_e^{\pi} \cdot BO_{ij}^{\pi} - D_e^{\pi\pi} \cdot BO_{ij}^{\pi\pi}$. Where D_e is the dissociation energy.

Lone Pair Electrons, Over-coordination, and Under-coordination. The energy penalty due to repulsion from lone pair electrons in the bonding is calculated based on the difference between the optimal number of lone pairs in an atom, $n_{lp,opt}$ and the number of lone pairs calculated, $n_{lp,i}$, from the difference between the number of outer shell electrons Val_i^e and the bond order.

$$\Delta_i^e = \sum_{j=1}^{neighbors} BO_{ij} - Val_i^e$$

$$n_{lp,i} = int\left(\frac{\Delta_i^e}{2}\right) + e^{-\lambda_8 \cdot (2 + \Delta_i^e - 2 \cdot int\left(\frac{\Delta_i^e}{2}\right))^2}$$

$$\Delta_i^{lp} = n_{lp,opt} - n_{lp,i}$$

$$E_{lp} = \frac{\lambda_9 \cdot \Delta_i^{lp}}{1 + e^{-75 \cdot \Delta_i^{lp}}}$$

The definition of over coordination gives that the energy penalty must be inversely proportional to the number of lone pairs present. A correction to the over coordination previously defined as Δ_i' can be made, Δ_i^{lpcorr}, using the deviation from the optimal lone pairs.

$$\Delta_i^{lpcorr} = \Delta_i' - \frac{\Delta_i^{lp}}{1 + \lambda_{10} \cdot e^{\lambda_{11} \cdot \left(\sum_{j=1}^{neighbors(i)}(\Delta_j' - \Delta_i^{lp}) \cdot (BO_{ij}^{\pi} - BO_{ij}^{\pi\pi})\right)}}$$

$$E_{ocoor} = \frac{\sum_{j=1}^{nbond} \lambda_{12} \cdot D_e^{\sigma} \cdot BO_{ij}}{\Delta_i^{lpcorr} + Val_i} \cdot \Delta_i^{lpcorr} \cdot \frac{1}{1 + e^{\lambda_{13} \cdot \Delta_i^{lpcorr}}}$$

Energy contribution from the under coordinated atoms is calculated based on the π electron in the atomic centers and is only calculated if the bonds between atom i and j have some π bond characteristics.

$$E_{ucoor} = -\lambda_{14} \cdot \frac{1 - e^{\lambda_{15} \cdot \Delta_i^{lpcorr}}}{1 + e^{-\lambda_{13}} \cdot \Delta_i^{lpcorr}} \cdot \frac{1}{1 + \lambda_{16} \cdot e^{\lambda_{17} \cdot (\Sigma_{j=1}^{neighbors(i)} (\Delta_j' - \Delta_i^{lp}) \cdot (BO_{ij}^\pi - BO_{ij}^{\pi\pi}))}}$$

Valence (Three-body) Angles. Valence angles are the three-body angles between atoms i, j, and k. To calculate the energy, E_{val}, of these three-body angles, Θ_{ijk}, we must first determine the equilibrium angle Θ_0, which depends on the sum of π-bond orders (SBO) around the center, considering the over and under coordination of the central atom and the lone electron pairs, changing the geometry of the center atom, and its neighbors. The valency of the atom used in the three-body and torsion angle calculations is denoted Val^{ang}. An energy penalty, E_{pen}, is imposed for systems with two double bonds sharing a central atom and for additional stability of complex systems, a three-body conjugation energy, E_{coa}, is also applied to the valence angles.

$$E_{val} = f_6(BO_{ij}) \cdot f_6(BO_{jk}) \cdot f_7(\Delta_j') \cdot (\lambda_{18} - \lambda_{18}e^{-\lambda_{19}(\theta_0(BO) - \theta_{ijk})^2})$$

$$f_6(BO_{ij}) = 1 - e^{-\lambda_{20} \cdot BO_{ij}^{\lambda_{21}}}$$

$$f_7(\Delta_j') = \lambda_{22} - (\lambda_{22} - 1) \cdot \frac{2 + e^{\lambda_{23} \cdot \Delta_j^{ang}}}{1 + e^{\lambda_{23} \cdot \Delta_j^{ang}} + e^{-\lambda_{24} \cdot \Delta_j^{ang}}}$$

$$\Delta_j^{ang} = \sum_{n=1}^{neighbors(j)} BO_{jn} - Val_j^{ang}$$

$$SBO = \sum_{n=1}^{neighbors(j)} (BO_{jn}^\pi + BO_{jn}^{\pi\pi}) + (1 - \prod_{n=1}^{neighbors(j)} (e^{-BO_{jn}^8})) \cdot (-\Delta_j^{ang} - \lambda_{25} \cdot n_{lp,j})$$

6

$$SBO_2 = \begin{cases} 0 & SBO \leq 0 \\ SBO^{\lambda_{26}} & 0 < SBO < 1 \\ 2 - (2 - SBO)^{\lambda_{26}} & 1 < SBO < 2 \\ 2 & SBO > 2 \end{cases}$$

$$\theta_0(BO) = \pi - \theta_{0,0} \cdot (1 - e^{-\lambda_{27} \cdot (2 - SBO_2)})$$

$$E_{pen} = \lambda_{28} \cdot f_8(\Delta'_j) \cdot e^{-\lambda_{29} \cdot (BO_{ij} - 2)^2} \cdot e^{-\lambda_{29} \cdot (BO_{jk} - 2)^2}$$

$$f_8(\Delta'_j) = \frac{2 + e^{-\lambda_{30} \cdot \Delta'_j}}{1 + e^{-\lambda_{30} \cdot \Delta'_j} + e^{\lambda_{31} \cdot \Delta'_j}}$$

$$E_{coa} = \lambda_{32} \cdot \frac{1}{1 + e^{\lambda_{33} \cdot \Delta_j^{val}}} \cdot e^{-\lambda_{34} \cdot \left(-BO_{ij} + \sum_{n=1}^{neighbors(i)} BO_{in}\right)^2} \cdot e^{-\lambda_{34} \cdot \left(-BO_{jk} + \sum_{n=1}^{neighbors(i)} BO_{kn}\right)^2}$$

$$\cdot e^{-\lambda_{35} \cdot (BO_{ij} - 1.5)^2} \cdot e^{-\lambda_{35} \cdot (BO_{jk} - 1.5)^2}$$

Torsion (Four-body) Angles. Much like the bond energies and valence angle terms, the torsion rotation energies, E_{tors}, are dependent on the BO. The effect of the four-body conjugation on the torsion angles, ω_{ijkl}, achieves a maximum value if multiple bonds have bond orders of 1.5.

$$E_{tors} = f_9(BO_{ij}, BO_{jk}, BO_{kl}) \cdot \sin(\theta_{ijk}) \cdot \sin(\theta_{jkl}) \cdot (\frac{1}{2} V_1 \cdot (1 + \cos(\omega_{ijkl})) + \frac{1}{2} V_2$$

$$\cdot e^{\lambda_{36} \cdot \left(BO_{jk}^{\pi} - 1 + f_{10}(\Delta'_j, \Delta'_k)\right)^2} \cdot (1 - \cos(2\omega_{ijkl}) + \frac{1}{2} V_3 \cdot (1 + \cos(3\omega_{ijkl}))$$

$$f_9(BO_{ij}, BO_{jk}, BO_{kl}) = (1 - e^{-\lambda_{37} \cdot BO_{ij}}) \cdot (1 - e^{-\lambda_{37} \cdot BO_{jk}})(1 - e^{-\lambda_{37} \cdot BO_{kl}})$$

$$f_{10}(\Delta'_j, \Delta'_k) = \frac{2 + e^{-\lambda_{38} \cdot (\Delta_j^{ang} + \Delta_k^{ang})}}{1 + e^{-\lambda_{38} \cdot (\Delta_j^{ang} + \Delta_k^{ang})} + e^{\lambda_{39} \cdot (\Delta_j^{ang} + \Delta_k^{ang})}}$$

$$E_{conj} = f_{11}(BO_{ij}, BO_{jk}, BO_{kl}) \cdot \lambda_{40} \cdot (1 + (\cos^2(\omega_{ijkl}) - 1) \cdot \sin(\theta_{ijk}) \cdot \sin(\theta_{jkl}))$$

$$f_{11}(BO_{ij}, BO_{jk}, BO_{kl}) = e^{-\lambda_{41} \cdot (BO_{ij} - \frac{3}{2})^2} \cdot e^{-\lambda_{41} \cdot (BO_{jk} - \frac{3}{2})^2} \cdot e^{-\lambda_{41} \cdot (BO_{kl} - \frac{3}{2})^2}$$

Hydrogen Bonds. The energy for the hydrogen bond X-H—Z, E_{Hbond}, uses the bond order, the valency angle of the central hydrogen atom, Θ_{XHZ}, and the radial distance between the atoms.

$$E_{Hbond} = \lambda_{42} \cdot (1 - e^{\lambda_{43} \cdot BO_{ij}}) \cdot e^{\lambda_{44} \cdot \left(\frac{r_{hb}^0}{r_{HZ}} + \frac{r_{HZ}}{r_{hb}^0} - 2\right)} \cdot \sin^8(\frac{\theta_{XHZ}}{2})$$

Van der Waals Interactions. The van der Waals energies, $E_{vdWaal,s}$ are calculated among all atoms, regardless of bonding and bond orders. A shielded interaction, $f_{12}(r_{ij})$, ensures that extreme repulsion between bonded and those atoms sharing a valence angle due to the van der Waals interactions does not occur. Also, to avoid discontinuities in the energy when going between bonded and non-bonded cutoffs, a Taper correction is included. The Taper correction takes form as a distance dependent 7th order polynomial where nonbonded energies and their derivatives are multiplied by the Taper terms, dependent on the non-bonded cutoff radii R_{cut} in the polynomial.

$$E_{vdWaals} = Tap \cdot D_{ij} \cdot (e^{\alpha_{ij}\left(1 - \frac{f_{12}(r_{ij})}{r_{vdW}}\right)} - 2 \cdot e^{\frac{1}{2}\cdot\alpha_{ij}\cdot\left(1 - \frac{f_{12}(r_{ij})}{r_{vdW}}\right)})$$

$$f_{12}(r_{ij}) = (r_{ij}^{\lambda_{44}} + \left(\frac{1}{\gamma_w}\right)^{\lambda_{44}})^{\frac{1}{\lambda_{44}}}$$

$$Tap = Tap_7 \cdot r_{ij}^7 + Tap_6 \cdot r_{ij}^6 + Tap_5 \cdot r_{ij}^5 + Tap_4 \cdot r_{ij}^4 + Tap_3 \cdot r_{ij}^3 + Tap_2 \cdot r_{ij}^2 + Tap_1 \cdot r_{ij}$$
$$+ Tap_0$$

$$Tap_7 = \frac{20}{R_{cut}^7}$$

$$Tap_6 = \frac{-70}{R_{cut}^6}$$

$$Tap_5 = \frac{84}{R_{cut}^5}$$

$$\text{Tap}_4 = \frac{-35}{R_{cut}^4}$$

$$\text{Tap}_{3-1} = 0$$

$$\text{Tap}_0 = 1$$

Coulomb Interactions. The energies due to coulombic interactions, $E_{coulomb}$, are also take all atom pairs into account using a shielded coulomb potential to adjust for orbital overlap between close atoms. The charges are calculated using the electron equilibration method (EEM) [18].

$$E_{coulomb} = \text{Tap} \cdot C \cdot \frac{q_i \cdot q_j}{(r_{ij}^3 + \left(\frac{1}{\gamma_{ij}}\right)^3)^{\frac{1}{3}}}$$

For a more comprehensive list of the parameters and their descriptions, see appendix A.

Force Fields for the Deposition of Alumina. The robustness of the ReaxFF methodology for reactive molecular dynamics is immediately evident from this brief review of the calculations used. Unfortunately, this robustness is offset by an increase in the number of trained parameters, λ_x, required and the computational accuracy of the training. Currently, the method for developing ReaxFF potentials requires the use of high accuracy quantum mechanical calculations wherein you take energies, bond lengths, charges, etc. for many orientations of your system and the ReaxFF parameters are fit against them. [19]. Another shortcoming of the ReaxFF method is transferability. After fitting a potential to a specific system, it is unlikely to be able to model even similar systems. It is because of this that a comprehensive review of the current ReaxFF potentials is needed. In this manuscript I will be describing the ability of two different available potentials. The first potential was developed by Hong et al [20] and the second was developed by Zheng et al [21], referred to by model 1 and model 2 going forward. Model 1 was developed to model the carbon coating of aluminum nanoparticles. A one parameter search

method was used, focusing on the reparameterization of the Al-C bond, and subsequently the Al-H bond was reparametrized as well. To fully describe these bonds, the EOS of aluminum carbide, adsorption, and decomposition energies for hydrocarbons on an aluminum surface cut to the (111) plane, and the dissociation energies of various Al-C-H-O clusters were included in the training set. The Al-O parameters were not included in the training [20]. Model 2 was developed to model the atomic layer deposition of alumina on hydroxylated and hydrogenated germanium (Ge) substrates. This potential was trained using EOS and formation energies of GeO and GeO_2, the bond distances and dissociation energies of the Ge-C, Ge-H, Ge-O, Ge=O, Al-C, and Al-Ge and angle distortion energies of H-Ge-O, C-Ge-O, Al-O-Ge, and O-Ge-O angles of clusters containing Ge/Al/C/O/H [21]. Understanding how these two differ in describing the ALD of alumina on aluminum is the first step toward developing a viable ReaxFF potential. The full potential files for model 1 and 2 is located in appendix B-1 and B-2 respectively.

COMPUTATIONAL METHODS

To thoroughly examine the capabilities of bother force fields several tests are performed. First the Al is confirmed to be stable by modeling the melting point, lattice parameter, and coefficient of thermal expansion (CTE) of both a crystal and a substrate of pure FCC Al. It is important to test both are stable because any deficiencies of the Al-Al bonds in the potentials for the crystal at higher temperatures could cause instability in the substrate at relatively lower temperatures. Next the precursors H_2O, TMA, DMA, and MMA are tested for stability and accuracy. Finally, the potentials are tested on the surface interactions that occur during the deposition process.

Crystal Substrate Stability

Crystal. A crystallography information file (CIF) primitive unit cell of FCC aluminum is obtained from the Material's Project database [22]. It is then replicated periodically to make a 20x20x20 supercell (32,000 atoms), and a visualization of the figure is made using OVITO [23] as seen in figure 1. MD simulations of the supercell are conducted using the LAMMPS ReaxFF software package [24]. A berendsen thermostat with a 0.25 fs time step is used to step the simulation through time. First, the crystal is relaxed under NPT (nonvariant pressure and temperature) at 300K for 10,000 steps (2.5 ps) with a pressure of 0 atm. It is then heated to 1050K at a rate of 0.08 K/fs. The volume is plotted against the temperature, and the melting point of the crystal is determined when the distribution becomes non-linear. The crystal is then relaxed at temperatures within the functional range of the ALD of alumina, 300K-600K every 25K for 2.5 ps. The lattice parameter, LP, is determined as a function of the volume $LP = (\frac{V}{20^3})^{\frac{1}{3}}$

and the coefficient of thermal expansion, CTE, as a function of the lattice parameters and temperature. $CTE_x = \frac{(LP_x - LP_i)}{LP_x(T_x - T_i)}$. The results are compared to each other and experimental results.
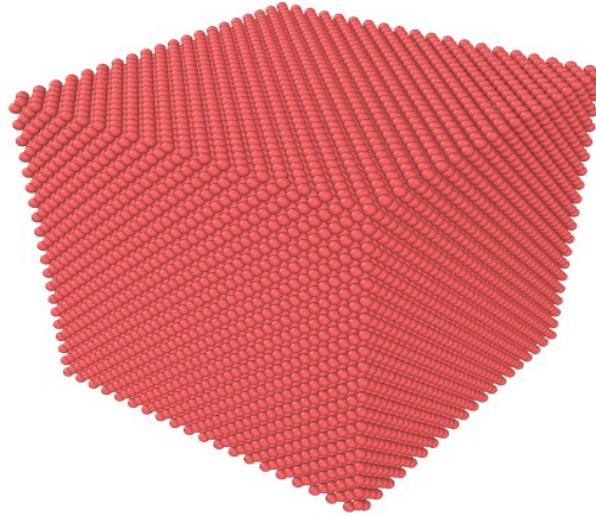
Figure 1: 20x20x20 supercell of aluminum crystal

Substrate. An Al(111) substrate 6 layers thick, 216 atoms, is generated using the USPEX [25] substrate generator as seen in figure 2. The substrate is heated from 100k to 1300K at a rate of 0.08 K/ps under NVT conditions. The melting point of the substrate is determined by plotting the energy against the temperature and by comparing the Al-Al radial distribution functions (RDF) between timesteps. The resulting melting points are then compared to each other and experimental results.
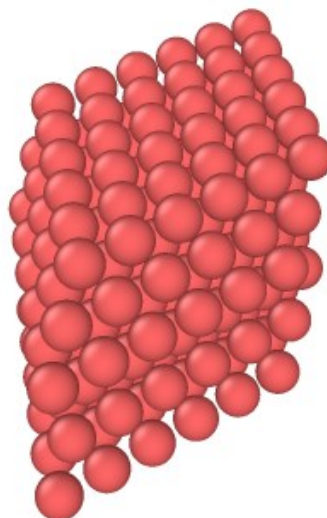
Figure 2: Al(111) substrate generated for verification of substrate stability

Precursor Stability

Reactive Force Field. Accuracy of the modeling of trimethylaluminum (TMA) is confirmed using a geometry optimization of a single molecule, figure 3a. The optmization was carried out at 0K using the BFGS quasi-Newtonian optimization method available on the Amsterdam Modeling Suites (AMS) [16, 19] platform. The optimization was performed to an energy convergence of 2.72×10^{-4} eV and a gradient convergence of 2.72×10^{-2} eV/Å. The bond distances for Al-C and C-H, and the angles for the H-C-H, C-Al-C, and Al-C-H are compared with experimental and DFT data. Identical relaxation was also performed for dimethylaluminum (DMA), figure 3b, and monomethylaluminum (MMA), figure 3c, as these precursor fragments are also abundant in the atomic layer deposition process.
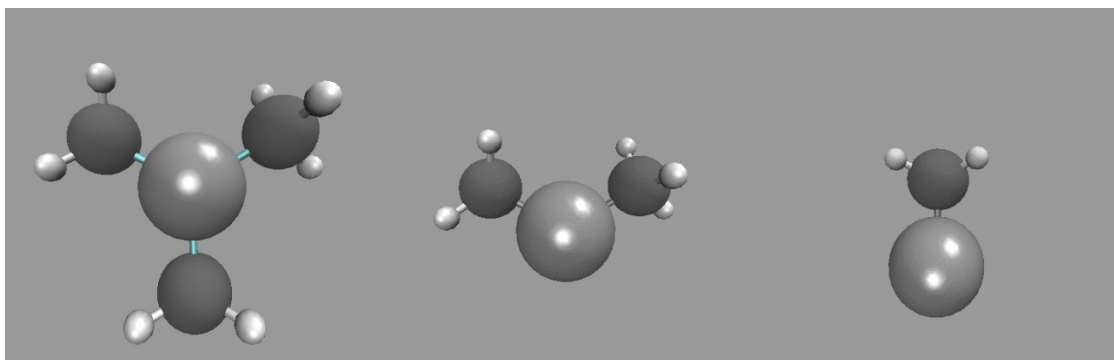
Figure 3: Snapshots of TMA (a) DMA (b) and MMA (c), Hydrogen-white, Carbon-dark grey, Al-light grey, before relaxation.

1000 H_2O molecules are packed into a cubic cell at a density of 1.5 g/cm^3 (figure 4), a higher density than that of water, using the PACKMOL [26] software. The cell is then relaxed under NPT conditions at 300K and 0 atm for 25 ps. The average volume and radial distributions of the O-H, O-O, and H-H are taken over the last 0.5 ps. The average lengths of the O-O and H-O bonds is also taken.

DFT Verification. Validation of the ReaxFF relaxations is done using the Vienna Ab initio Simulation Package (VASP) [27]. The PBE [28] functional in the projector augmented wave (PAW) [29] method is used. An energy cutoff of 520 eV with gaussian smearing (σ=0.05 eV) and a 1x1x1 k-point grid is automatically generated using the Monkhorst package [30]. The geometry optimizations are done to an energy convergence of $1x10^{-5}$ eV and an ionic convergen ce of $1x10^{-4}$.

Reaction Pathway Modeling

Reactive Force Field. In an effort to determine the ability of each force field to model the ALD process, 3 scenarios are taken into account. The initial adsorption of a TMA onto a

wetted Al(111) surface, the first ligand exchange of the H_2O pulse, and the second ligand exchange of the H2O pulse. The energy pathways of these scenarios are determined through geometry optimization and compared to DFT results to determine any deficiencies in the potentials.
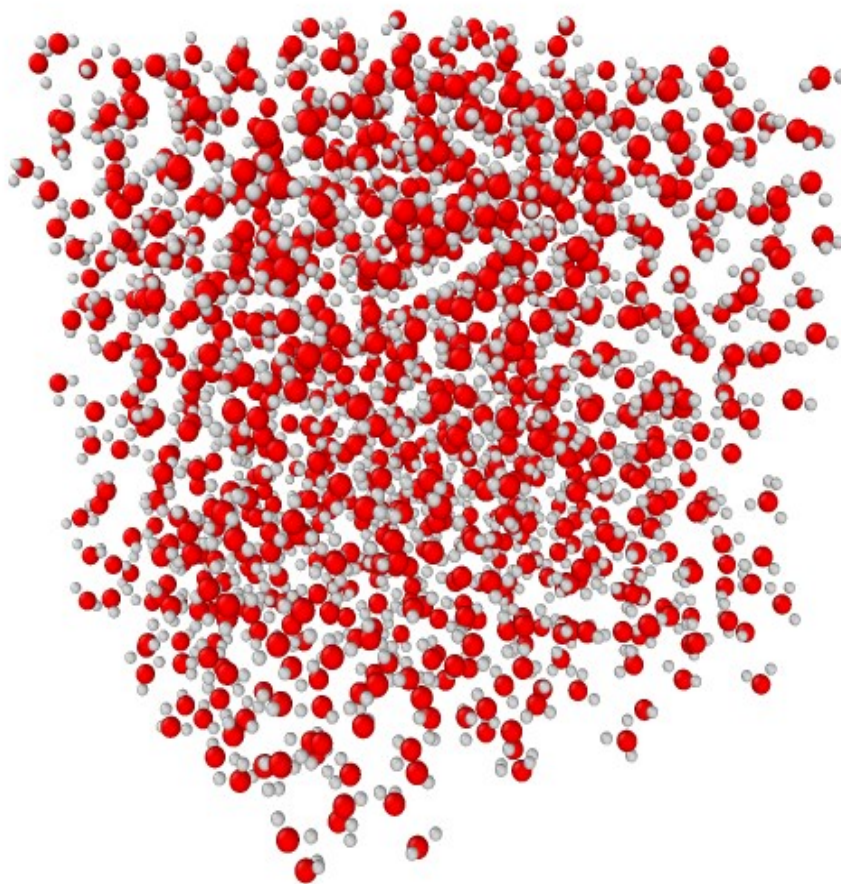
Figure 4: H_2O, H-white O-red, packed into a cubic volume

Adsorption of TMA on a Wetted Al(111) Surface. A 3 layer 2x2 of Al(111), 109 Al atoms, is generated. A single hydroxyl unit is allowed to relax on the surface of the substrate and a single, unbonded TMA is introduced into the system. This is taken as the first state of the TMA

adsorption, figure 5a. The second state of the system is the adsorption of the TMA onto the

hydroxyl unit, figure 5b, then the ligand exchange is modeled by the bond breaking and

formation of the hydrogen from the hydroxyl unit to one of the methyl units of the TMA. This

transitional state of the methane (CH_4) formation before desorption is the third state, figure 5c.

The final state of the system is taken after the desorption of the methane from the surface, figure

5d. The geometeries of all the states are optimized with an energy convergence of $2.72x10^{-4}$ eV

and a gradient convergence of $2.72x10^{-2}$ eV/Å and are checked for non-physical geometries to

ensure the accuracy of the relaxation.

Adsorption of the First H_2O onto DMA. To model the adsorption of the first H_2O

adsorption, the methane product is purged from the final state of the TMA adsorption, and a

single H_2O molecule is added to the system, figure 6a. Then the adsorption of the H_2O is

modeled, figure 6b, and the ligand exchange transition state, 6c. Finally, the methane desorption

is modeled, 6d, and all geometries were optimized with an energy convergence of $2.72x10^{-4}$ eV

and a gradient convergence of $2.72x10^{-2}$ eV/Å.

Adsorption of the Second H_2O onto MMA. The second H_2O adsorption is modeled

similarly to the first. The methane is purged and a single H_2O molecule is added to the system

(figure 7a), then the adsorption state (figure 7b), transition state (figure 7c), and the desorption of

the methane (figure 7d) are modeled. All the geometries are then optimized under the same

conditions.

DFT Verification. To determine the accuracy of the reaction pathways determined by

using the ReaxFF geometry optimization, DFT calculations are performed using the VASP

software. Because these are surface interactions involving multiple molecules, the inclusion of

the Van der Waals (VdW) forces into the DFT calculations is necessary.
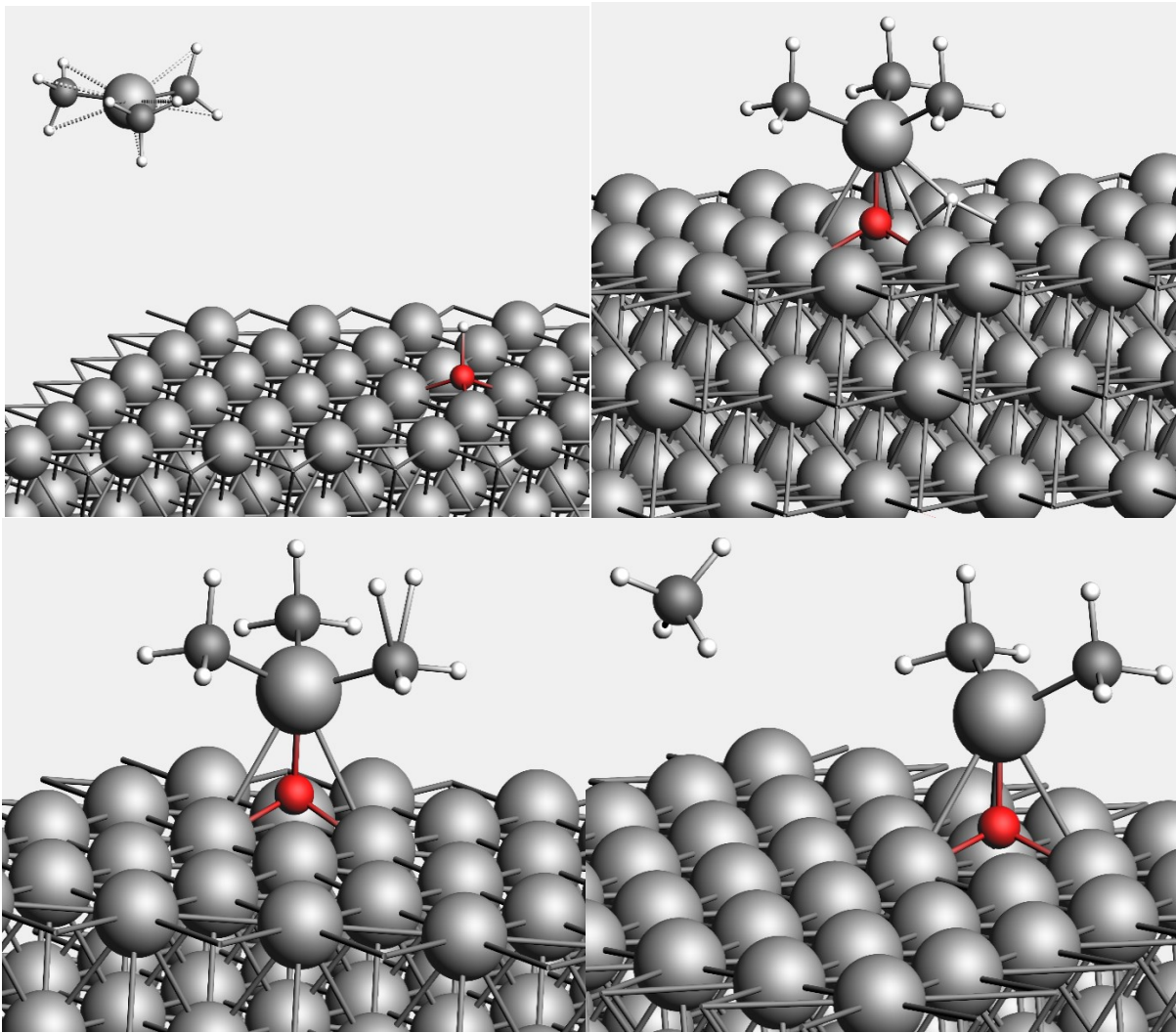
Figure 5: TMA adsorption onto wetted Al intial (a) adsorption (b) transition (c) and desorption (d) states.

Van der Waals play a critical role in intermolecular interactions and adsorption mechanics [31]. VdW calculations are included using the VdW kernel available at VASP [32-34]. Geometry optimizations of all states are performed and the energies relative to the initial state are used to determine the energy barrier for the transition states and the overall energy change of the reaction path. These energies are compared to the energies of both models to evaluate their ability to describe the system.
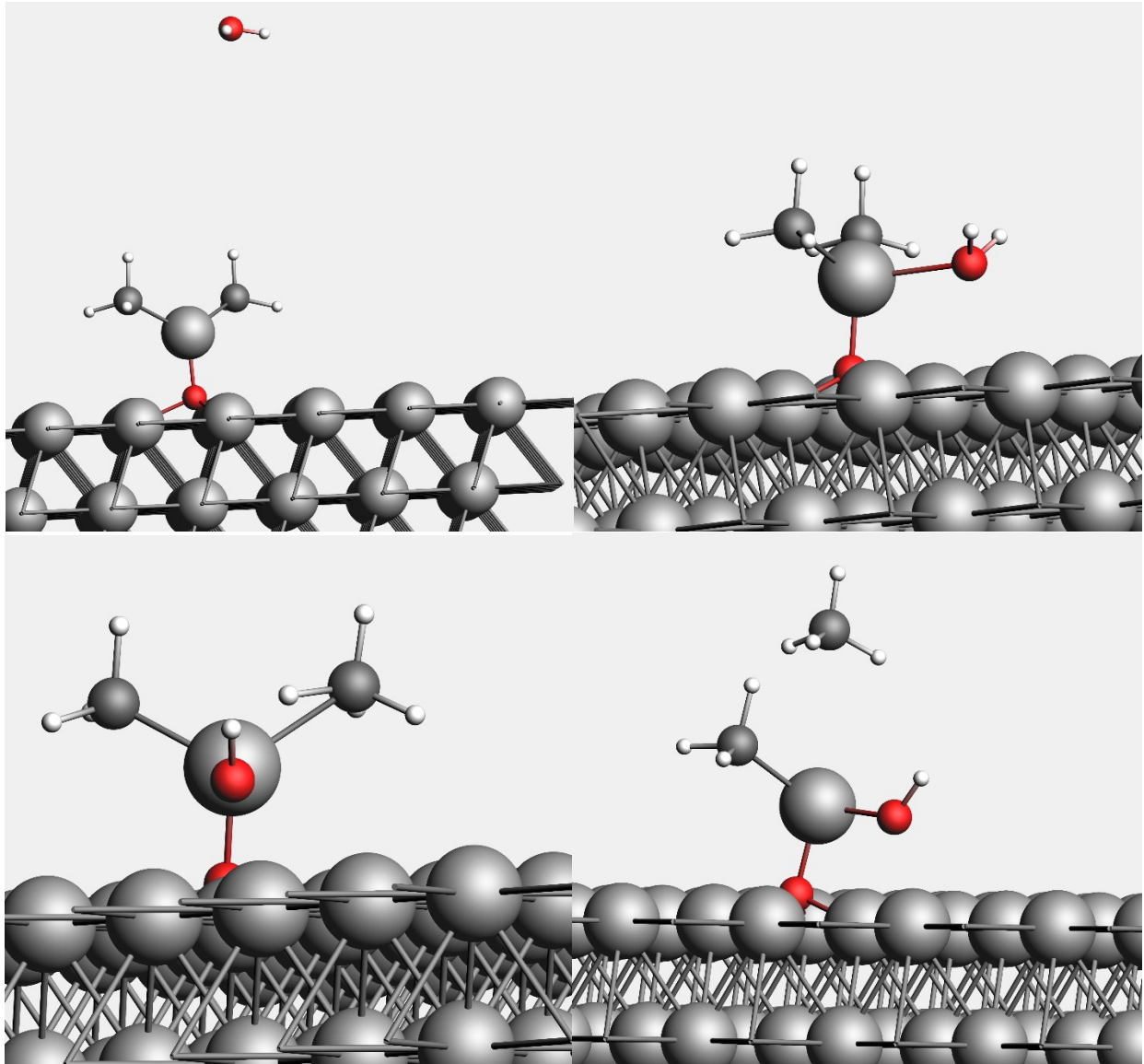
Figure 6: H₂O adsorption onto DMA intial (a) adsorption (b) transition (c) and desorption (d) states.

The geometry optimizations were done with the PBE functional in the PAW method are used. An energy cutoff of 300 eV with gaussian smearing (σ=0.05 eV) and a 1x1x1 k-point grid are automatically generated using the Monkhorst package and an energy convergence of $1x10^{-3}$ eV and ionic force convergence of $1x10^{-2}$.
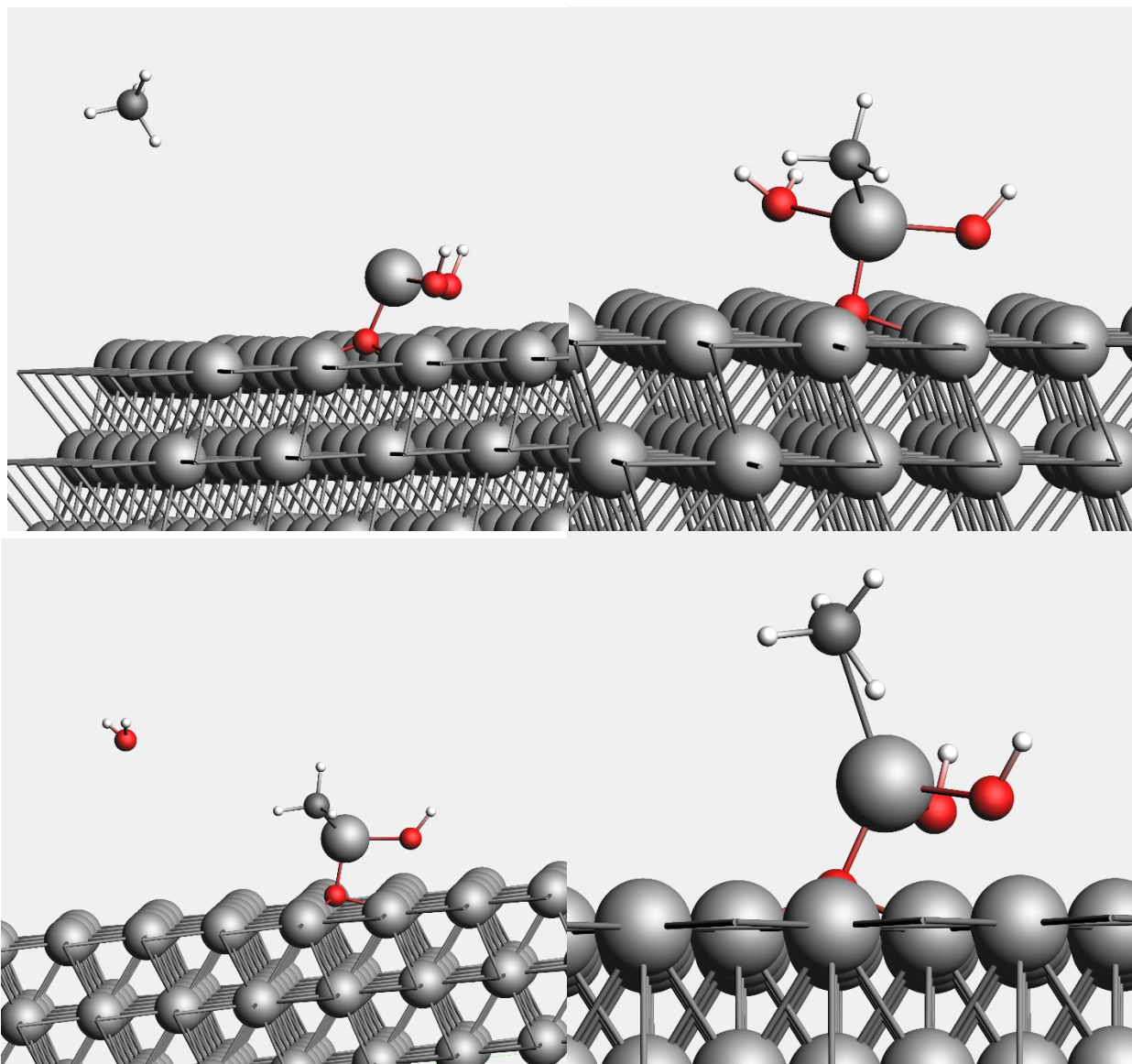
Figure 7: H$_2$O adsorption onto MMA intial (a) adsorption (b) transition (c) and   desorption (d) states.

Crystal and Substrate Stability

   Crystal Stability. After relaxation, the crystal volume was plotted against the temperature for model 1 and model 2, figures 8a and 8b respectively. The melting point of the crystal is determined from the point of the distribution that becomes non-linear. The lattice parameters and coefficients of thermal expansion are calculated from the volumes at temperatures ranging from 300 to 600 every 25 K, table 1.
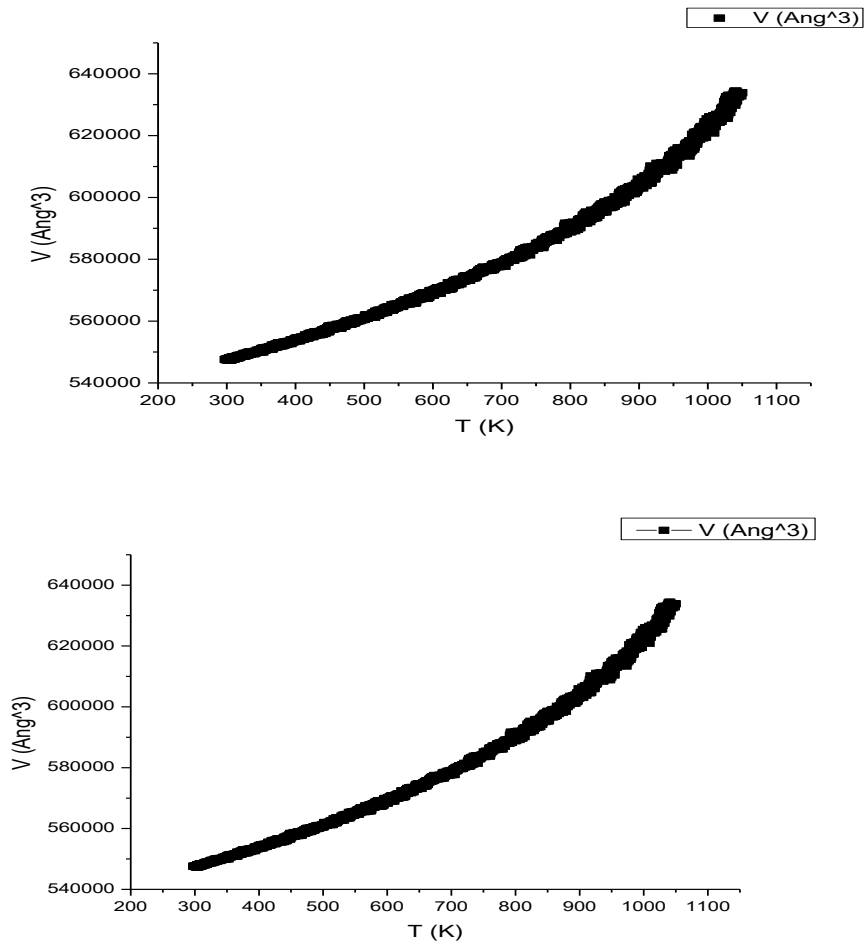
Figure 8: Volume ($Å^3$) and Temperature (K) of Al crystal for model 1 (a) and model 2 (b)

Table 1: Volume, lattice parameter and CTE of Al crystals at temperatures ranging from 300 K to 600 K for model 1 and 2

	Model 1			Model 2		
T (K)	V (x10^{-5} Å^3)	LP (Å)	CTE (x10^6 K^{-1})	V (x10^{-5} Å^3)	LP (Å)	CTE (x10^6 K^{-1})
300	5.47465	4.090302113		5.47475	4.090328634	
325	5.48946	4.093987854	36.04371065	5.48964	4.094033146	36.22704137
350	5.50585	4.098058005	37.92332363	5.50566	4.098011051	37.56381333
375	5.52183	4.102019038	38.19416577	5.52159	4.101959454	37.91323853
400	5.53827	4.106085619	38.58762916	5.5381	4.106044607	38.42227556
425	5.55557	4.110356104	39.22251413	5.55547	4.110331486	39.12224002
450	5.57316	4.114690404	39.74977997	5.57314	4.114685295	39.69796939
475	5.59125	4.119136495	40.28257417	5.59137	4.11916683	40.2876412
500	5.61062	4.123889592	41.05745504	5.61028	4.123805491	40.92196528
525	5.63007	4.128649103	41.66711017	5.62973	4.128565225	41.54688295
550	5.65007	4.133532622	42.27610426	5.65012	4.133543342	42.26037766
575	5.67125	4.138689656	43.01753248	5.67117	4.138671732	42.97774083
600	5.69352	4.144100504	43.84223125	5.69314	4.144007843	43.74482208

The values of the melting points, lattice parameters at 400K and coefficients of thermal expansion are included in table 2 and compared against experimental results from Nakashima et al. [35].

Table 2: Comparison of the MP, LP, and CTE of model 1 and 2 with experimental data from Nakashima et al.

	Al Crystal Melting Point (K)	Al Crystal Lattice Parameter @ 400 K (Å)	CTE ($\times 10^6$ K^{-1}) @ 600 K
Model 1	910	4.106	43.37
Model 2	910	4.106	43.37
Nakashima	933	4.059	28.03
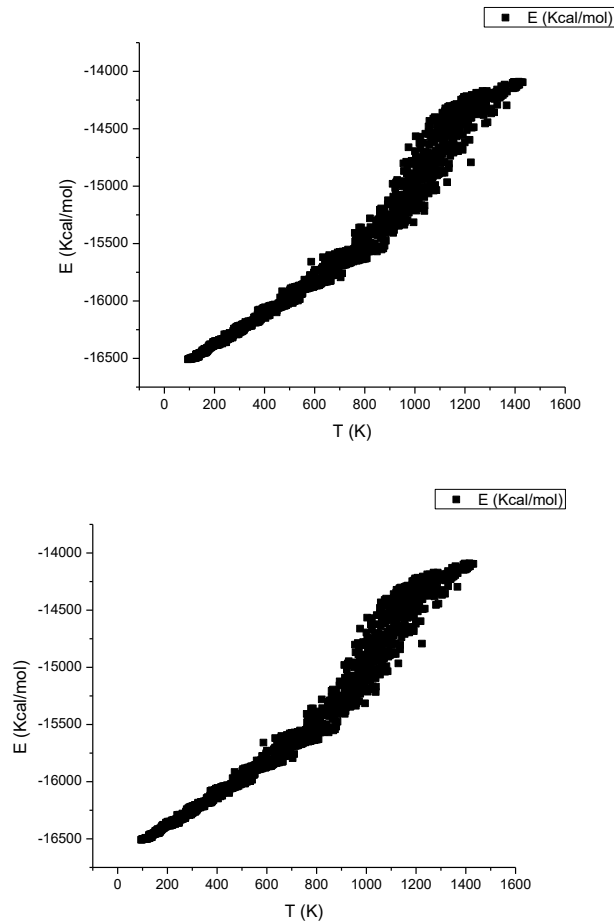
Figure 9: Energy (Kcal/mol) vs temperature (K) for Al(111) substrate model 1 (a) and model 2 (b)
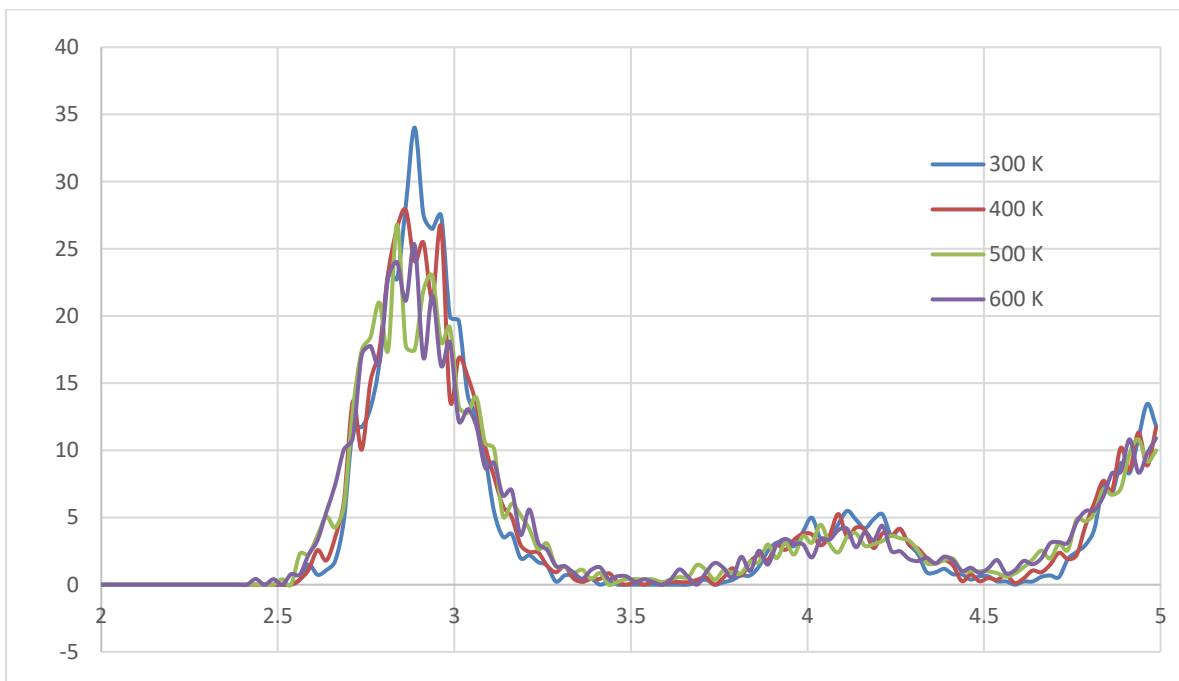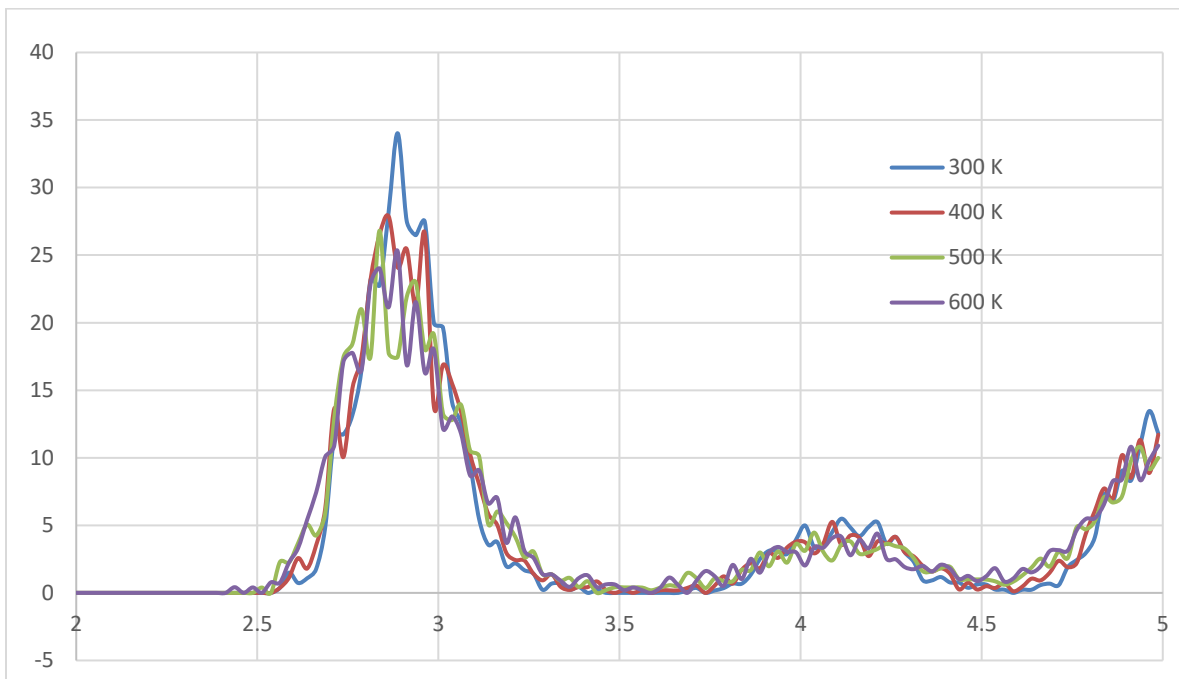
Figure 10: The Al-Al radial distribution functions at 300 K, 400 K, 500 K, and 600 K for model 1 (a) and model 2 (b)

Substrate Stability. After heating the Al(111) substrate to about 1300 K, the effective melting point of the substrate is determined by an incontinuity in the distribution of the potential energy of the system versus the temperature, figures 9a and 9b for models 1 and 2 respectively. The Al-Al RDF's for temperatures ranging from 300 K-600 K are presented in figures 10a and 10b.

Precursor Stability

TMA. Table 3 shows the results of the relaxations for TMA, DMA, and MMA molecules for model 1, model 2, and DFT calculations.

Table 3: Relaxation values for TMA, DMA, and MMA molecules for model 1, model 2, and DFT calculations.

	TMA					DMA					MMA			
	Al-C (Å)	C-H (Å)	C-Al-C (Θ)	H-C-H (Θ)	Al-C-H (Θ)	Al-C (Å)	C-H (Å)	C-Al-C (Θ)	H-C-H (Θ)	Al-C-H (Θ)	Al-C (Å)	C-H (Å)	H-C-H (Θ)	Al-C-H (Θ)
Model 1	1.97	1.17	120	108.9	110	1.96	1.17	115.9	109.2	109.8	1.96	1.17	109.2	109.7
Model 2	1.94	1.17	120	111.4	107.5	1.93	1.17	130.3	111.5	107.4	1.92	1.16	112	106.9
DFT	1.97	1.10	119.99	106.94	111.88	1.98	1.11	117.91	108.17	110.70	1.99	1.11	106.96	111.88

H$_2$O. The average volume of the last 0.5 ps of the ReaxFF molecular dynamics gave densities of water of 0.859 g/cm^3 for model 1 and 0.856 g/cm^3 for model 2. Figure 11a-d shows the g(r)'s for the bulk water compared to results published by LaCount et al [36] and table 4

contains the average O-O and O-H bond lengths and densities for model 1 and model 2

compared to results published by Sun et al. [37].
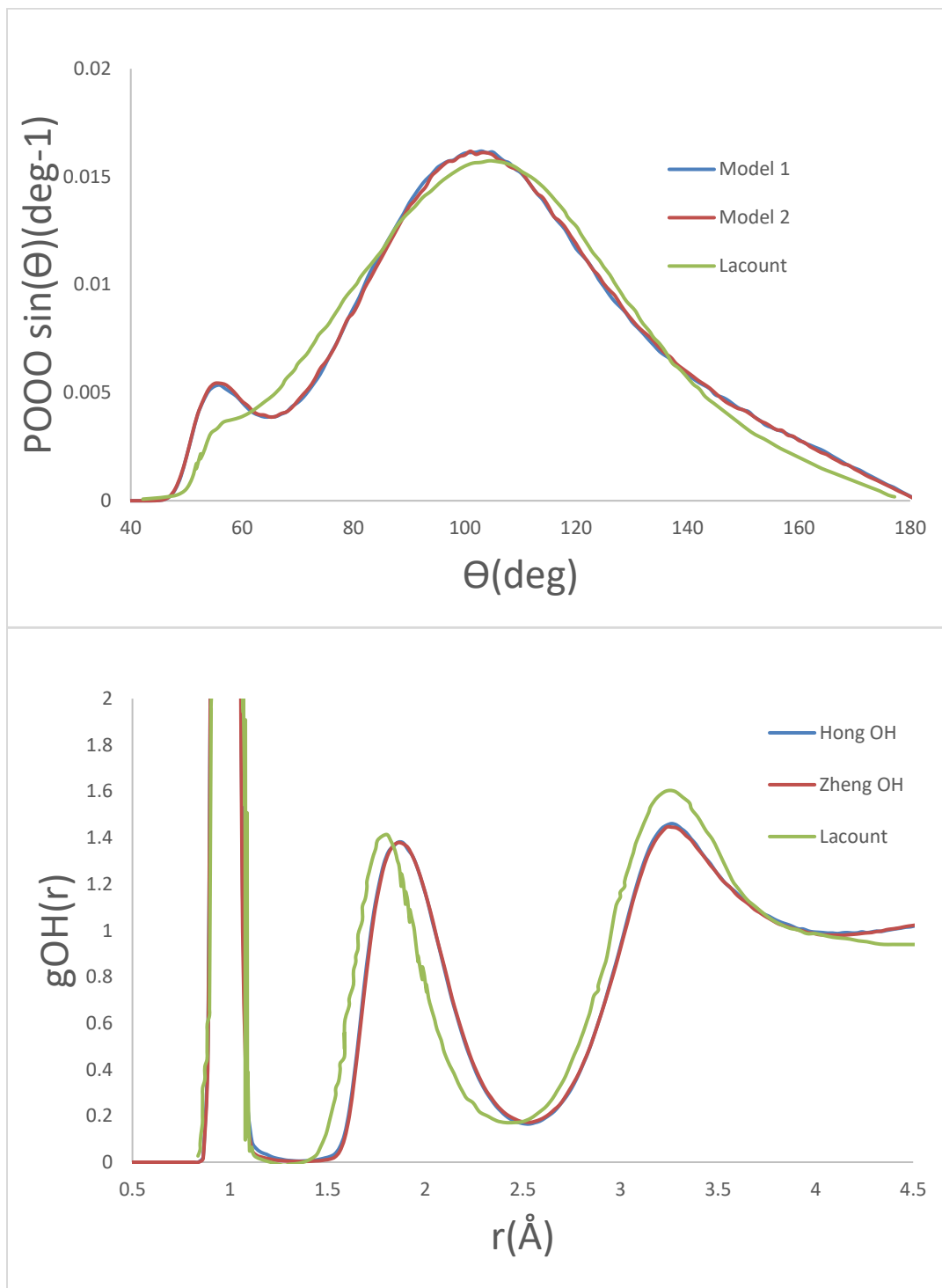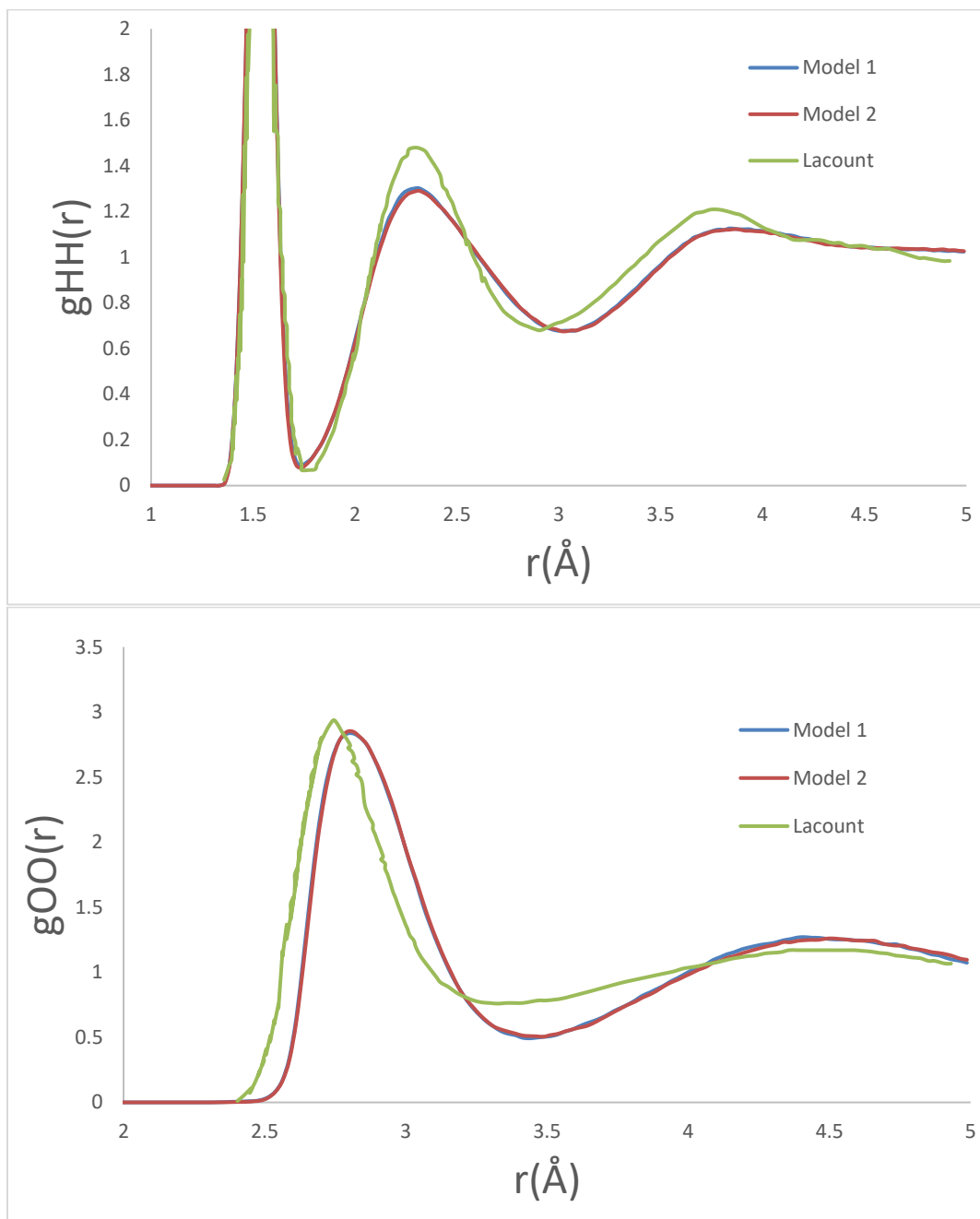
Figure 11: ReaxFF O-O-O angle (a), g(r) for O-H (b), H-H (c), and O-O (d) compared to data from Lacount et al.

Table 4: Density and average bond lengths of relaxed cell of water for model 1 and model 2 compared to results published by Sun et al.

	Density (g/cm^3)	O-O (Å)	O-H (Å)
Model 1	0.858921	2.86	0.967
Model 2	0.855628	2.83	0.967
Sun et al.	0.999987	2.7	0.97-1.01

Reaction Pathway Energies

  TMA Adsorption to Wetted Al(111) Surface. The pathway for the reaction of TMA with a wetted aluminum surface for each of the models is compared to DFT calculations performed, figure 12.
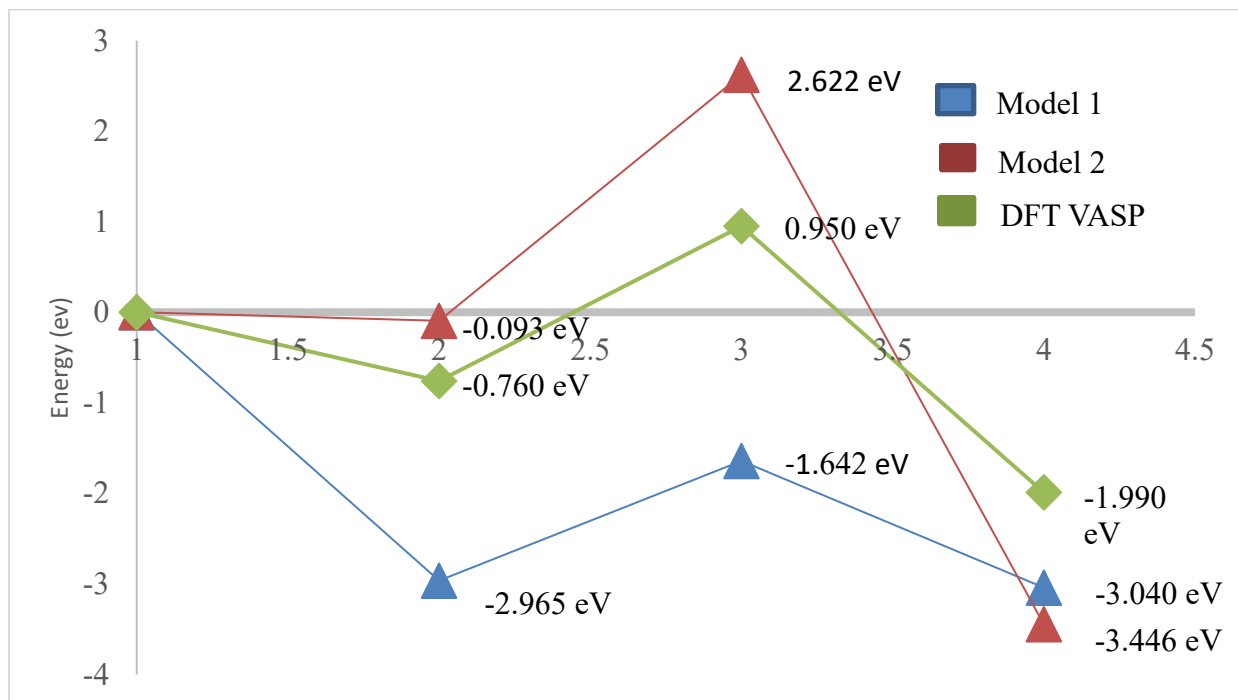
Figure 12: Energy path for model 1, model 2, and DFT calculations of TMA reacting with wetted surface.

First H₂O Adsorption to Terminating DMA. The pathway for the reaction of H_2O onto a terminating DMA for each of the models is compared to DFT calculations performed, figure 13.

Second H₂O Adsorption to Terminating MMA. The pathway for the reaction of H_2O onto a terminating MMA-OH for each of the models is compared to DFT calculations performed, figure 14.

Charges

Table 5 a-c shows the charges for the adsorbed aluminum and interstitial oxygen for the pre-adsorption, adsorption, and methane desorption states of the initial TMA deposition and two subsequent H_2O reactions.
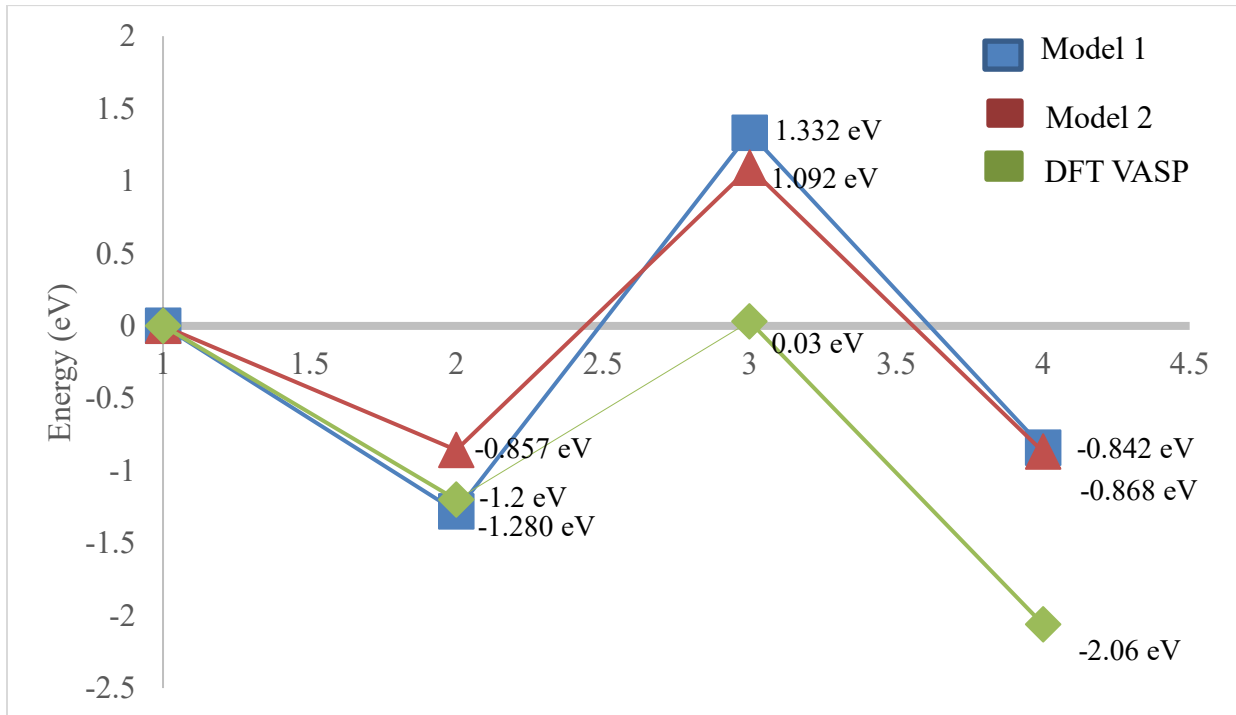
Figure 13: Energy path for model 1, model 2, and DFT calculations of H_2O reacting with a terminating DMA.
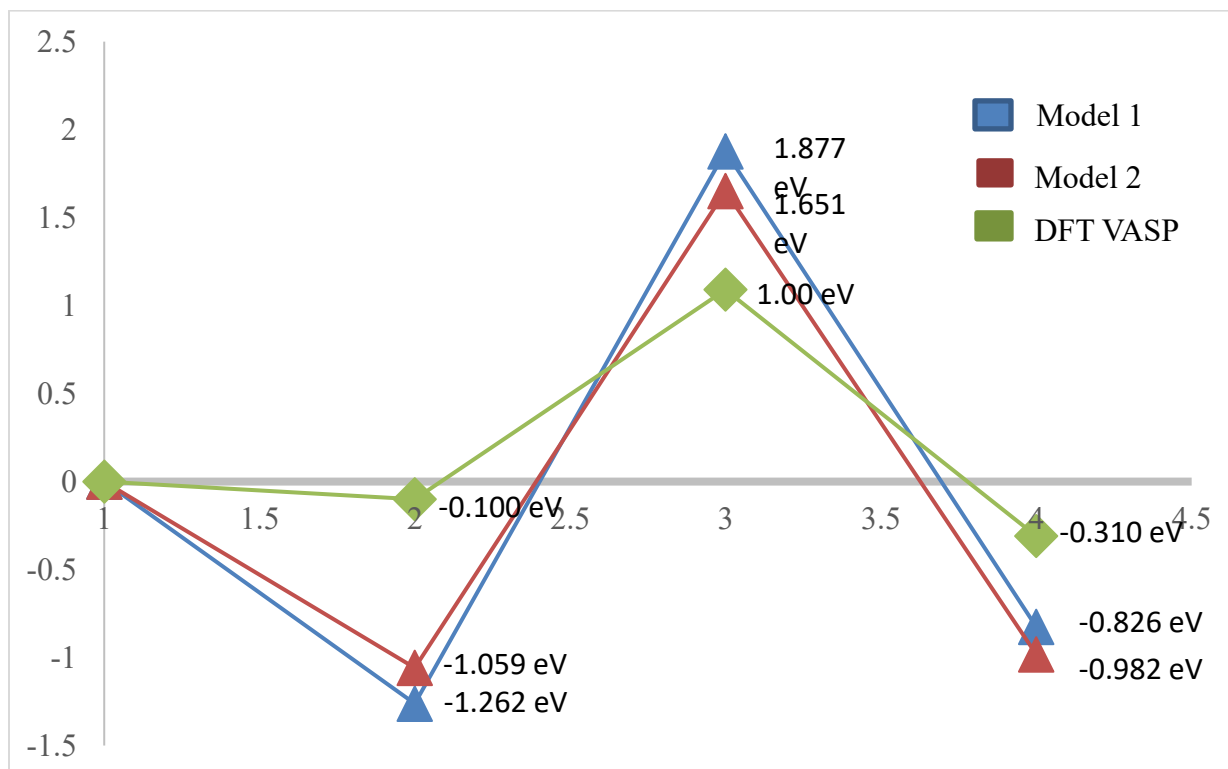
Figure 14: Energy path for model 1, model 2, and DFT calculations of H_2O reacting with a terminating MMA-OH.

Table 5a: Adsorbed Al and interstitial O charges for initial TMA adsorption of model 1 and 2

	Model 1			Model 2		
	Pre-adsorption	Adsorption	Methane Desorption	Pre-adsorption	Adsorption	Methane Desorption
Al	0.8361	1.0114	0.8205	0.8578	1.0681	0.8051
O	-0.8881	-1.0063	-1.0397	-0.8190	-0.8209	-1.0305

Table 5b: Adsorbed Al and interstitial O charges for first H2O adsorption of model 1 and 2

	Model 1			Model 2		
	Pre-adsorption	Adsorption	Methane Desorption	Pre-adsorption	Adsorption	Methane Desorption
Al	0.8164	0.9953	0.8917	0.8075	0.9774	0.8425
O	-1.0389	-1.0442	-1.0415	-1.0292	-1.0297	-1.0450

Table 5c: Adsorbed Al and interstitial O charges for second H_2O adsorption of model 1 and 2

	Model 1			Model 2		
	Pre-adsorption	Adsorption	Methane Desorption	Pre-adsorption	Adsorption	Methane Desorption
Al	0.8844	1.0866	0.9597	0.8245	1.0095	0.8884
O	-1.0398	-1.0428	-1.0428	-1.0428	-1.0516	-1.0546

DISCUSSION

Crystal, Surface, and Precursors

After the relaxation of the 20x20x20 crystal of FCC aluminum, the melting point of both model 1 and model 2 are calculated to be approximately 910 K. This result is in good agreement with experimental values. The lattice parameters and coefficients of thermal expansion for both models are also in agreement, 4.106 Å and 43.37×10^{-6} K^{-1} respectively. The coefficient of thermal expansion calculated from the potentials is twice that of the known CTE of aluminum (approximately 28.03×10^{-6} K^{-1}). This with the 0.047 Å lattice parameter and 23 K differences indicate that the Al-Al two, three, and four bonds are weaker than expected. No instability is evident in the volume of the crystals within the effective deposition temperature range. The testing of the substrates yields similar results. The Al(111) substrates for models 1 and 2 are stable, linear increase in energy indicating no amorphous characteristics within the substrate, within the deposition temperature range of 300 K-600 K. The radial distribution functions show no widening of the peaks between the temperature range, another indication of stability, and the average first nearest neighbor Al-Al bond length of 2.89 Å is in good agreement with values cited by Preobrajenski [38].

The g(r)'s for the bulk water at 300 K show a lengthening of the O-O peak by approximately 0.1 Å and the second nearest neighbor O-H peak by 0.14 Å to the experimental data. This is indicative of a widening of the bonds between the H_2O molecules. The lower densities of both model 1 and model 2, 0.859 g/cm^3 and 0.856 g/cm^3 respectively, show potential weakening in the hydrogen bonding that causes the cohesiveness between water molecules. The O-H first nearest neighbor peak and the O-O-O angle distribution also matches closely agree with the experimental data.

The average TMA Al-C bond length for model 1 matches the DFT calculations and previous studies by Berthomieu et al. [39] and Almenningen et al. [40]. Model 2 has an Al-C bond length that is approximately 0.03 Å less than the accepted value. This difference in the Al-C bond between the DFT calculations and model 2 increases as the methyl ligands of the precursor as removed. While the DFT calculations indicate that the bond length should increase as the Al loses its methyl bonds, the bond lengths for model 1 remain stagnant and model 2 decrease. The TMA C-H bond length for both models agreed at 1.17 Å, 0.07 Å more than the DFT calculations and data from Berthomieu and Almenningen. This is a pattern that is seen repeated for the DMA and MMA C-H bond lengths. This indicates that the hydrogen bond lengths are extended in the C-H bonds as well as the O-H bonds. The Al-C-H and H-C-H angle measurements for model 1 are equal and are consistent between the TMA, DMA, and MMA precursors. Model 2 has a higher H-C-H angle than Al-C-H, the inverse of the DFT results. This is also persistent between TMA, DMA, and MMA. This could indicate that the valency and/or bond order parameters are not fit well for the precursors. It is important to note that model 1 modeled the angles and bond lengths of the precursor more accurately than model 2, surprising considering model 2 used TMA as a molecule in its training.

The Reactions

TMA Adsorption on a Hydroxylated Al(111) Surface. The initial adsorption energy for model 2 was almost zero. This indicates that spontaneous adsorption of TMA onto the hydroxylated surface may not be seen or may not be very frequent using model 2. The energy barrier of 2.715 eV is 1 eV more than the DFT calculation of 1.71 eV energy barrier. This indicates that the Al-C bond after the TMA is attracted to the H does not lengthen, allowing for

the ligand exchange to the now weakened methyl unit and the formation of methane. These results are consistent with the precursor stability test. The reaction pathway for Model 1 shows a greater loss in energy after adsorption and a lower energy barrier (1.323 eV), but the overall loss in energy is approximately equal to the adsorption energy which means the ligand exchange is not as favorable.

H_2O Adsorption onto Surface DMA. The reaction pathway for the adsorptions of first and second H_2O for both models show an Al-O bond is formed spontaneously (-1.28 eV and -0.857 eV ΔE for model 1 and 2 respectively). Overall change in energy of the reactions indicates an exothermic reaction and are -0.852 eV for model 1 and -0.868 eV for model 2. The energy barrier for the transition states is 2.612 eV for model 1 and 1.949 eV for model 2. The relative energy after the desorption of the methane for model 1 is not lower than the energy after the initial adsorption, which indicates the ligand exchange will not occur for the second interaction of the deposition process either. This could be due to a decreased dissociation energy of the Al-C that is evident in the potential (Appendix B-1). Model 2 on the other hand ends on a lower energy than the initial adsorption (0.011 eV lower) but has a higher energy barrier than the DFT calculation. This indicates there will be a spontaneous adsorption and favorable formation of methane, which is noted in the results published in Zheng et al. [21].

H_2O Adsorption onto Surface MMA-OH. The second H_2O adsorption for both models is spontaneous with an adsorption energy of -1.262 eV for model 1 and -1.059 eV for model 2. Both models sport a high energy barrier (3.139 eV for model 1 and 2.71 eV for model 2) and lower desorption energy of the methane. This means that the ligand exchange and formation of the terminating Al-2OH for the H_2O pulse of the atomic layer deposition of alumina are not favorable to occur.

CONCLUSIONS

The current ReaxFF potentials can model a stable Al surface and bulk water. Model 1 can model the TMA precursor and its decomposition fairly well. It fails to simulate the surface reactions of the ALD process, though, likely due to lower dissociation energy of the Al-C bond leading to stronger bonding between the central Al atom of TMA and the C of the methyl unit. Model 2 does not model TMA or its decompositions well. Shortening of the Al-C bond lengths after decomposition and lower Al-C-H bond lengths are indications that the bond orders for the C valency and torsion terms. Model 2 did, however, show evidence of spontaneous adsorption and favorable formation and desorption of methane during the first H_2O deposition, showing that describing the individual precursor is not necessarily a prerequisite of modeling the system. Reparameterization of the currently available ReaxFF potentials is necessary in order to model the ALD of alumina on an aluminum surface. The training set should include the bond orders, dissociation energies, and valencies of molecules containing Al-C-H-O. Although this could be a rigorous process, the number of data points needed could be reduced by utilizing techniques in artificial intelligence and machine learning.

REFERENCES

(1) Lapham, P.; Georgiev, V. Computational study of oxide stoichiometry and variability in the Al/AlOx/Al tunnel junction. *Nanotechnology* **2022**. DOI: 10.1088/1361-6528/ac5f2e.

(2) Müller, C.; Cole, J. H.; Lisenfeld, J. Towards understanding two-level-systems in amorphous solids: insights from quantum circuits. *Rep. Prog. Phys.* **2019**, *82* (12), 124501. DOI: 10.1088/1361-6633/ab3a7e.

(3) Bilmes, A.; Volosheniuk, S.; Ustinov, A. V.; Lisenfeld, J. Probing defect densities at the edges and inside Josephson junctions of superconducting qubits. *npj. Quantum Inf.* **2022**, *8* (1). DOI: 10.1038/s41534-022-00532-4.

(4) Cyster, M. J.; Smith, J. S.; Vogt, N.; Opletal, G.; Russo, S. P.; Cole, J. H. Simulating the fabrication of aluminium oxide tunnel junctions. *npj. Quantum Inf.* **2021**, *7* (1). DOI: 10.1038/s41534-020-00360-4.

(5) DuBois, T. C.; Cyster, M. J.; Opletal, G.; Russo, S. P.; Cole, J. H. Constructingab initiomodels of ultra-thin Al–AlOx–Al barriers. *Mol. Simul.* **2015**, *42* (6-7), 542-548. DOI: 10.1080/08927022.2015.1068941.

(6) Elliot, A. J.; Malek, G.; Wille, L.; Lu, R.; Han, S.; Wu, J. Z.; Talvacchio, J.; Lewis, R. M. Probing the Nucleation of $\hbox{Al}_{2}\hbox{O}_{3}$ in Atomic Layer Deposition on Aluminum for Ultrathin Tunneling Barriers in Josephson Junctions. *IEEE Trans. Appl. Supercond.* **2013**, *23* (3), 1101405-1101405. DOI: 10.1109/tasc.2013.2247452.

(7) Shen, D.; Zhu, R.; Xu, W.; Chang, J.; Ji, Z.; Sun, G.; Cao, C.; Chen, J. Character and fabrication of Al/Al2O3/Al tunnel junctions for qubit application. *Sci. Bull.* **2012**, *57* (4), 409-412. DOI: 10.1007/s11434-011-4821-4.

(8) Xie, Y.; Pan, D.; Ma, L.; Yuan, C. Optimizing the process efficiency of atomic layer deposition of alumina for its sustainability improvement: a combined experimental and modeling study. *J. Clean. Prod.* **2016**, *133*, 338-347. DOI: 10.1016/j.jclepro.2016.05.138.

(9) George, S. M. Atomic layer deposition: an overview. *Chem. Rev.* **2010**, *110* (1), 111-131. DOI: 10.1021/cr900056b.

(10) Puurunen, R. L. Surface chemistry of atomic layer deposition: A case study for the trimethylaluminum/water process. *J. Appl. Phys.* **2005**, *97* (12). DOI: 10.1063/1.1940727.

(11) Groner, M. D.; Elam, J. W.; Fabreguette, F. H.; George, S. M. Electrical characterization of thin Al2O3 films grown by atomic layer deposition on silicon and various metal substrates. *Thin Solid Films* **2002**, *413* (1-2), 186-197. DOI: 10.1016/s0040-6090(02)00438-8.

(12) Higashi, G. S.; Fleming, C. G. Sequential surface chemical reaction limited growth of high quality Al2O3dielectrics. *Appl. Phys. Lett.* **1989**, *55* (19), 1963-1965. DOI: 10.1063/1.102337.

(13) Soto, C.; Tysoe, W. T. The reaction pathway for the growth of alumina on high surface area alumina and in ultrahigh vacuum by a reaction between trimethyl aluminum and water. *J. Vac. Sci. Technol. A* **1991**, *9* (5), 2686-2695. DOI: 10.1116/1.577226.

(14) Strempel, V. E.; Knemeyer, K.; Naumann d'Alnoncourt, R.; Driess, M.; Rosowski, F. Investigating the Trimethylaluminium/Water ALD Process on Mesoporous Silica by In Situ Gravimetric Monitoring. *Nanomaterials* **2018**, *8* (6). DOI: 10.3390/nano8060365.

(15) Goul, R.; Wilt, J.; Acharya, J.; Liu, B.; Ewing, D.; Casper, M.; Stramel, A.; Elliot, A.; Wu, J. Z. Electron tunneling properties of Al2O3 tunnel barrier made using atomic layer deposition in multilayer devices. *AIP Adv.* **2019**, *9* (2). DOI: 10.1063/1.5052163.

(16) Chenoweth, K.; van Duin, A. C.; Goddard, W. A., 3rd. ReaxFF reactive force field for molecular dynamics simulations of hydrocarbon oxidation. *J. Phys. Chem. A* **2008**, *112* (5), 1040-1053. DOI: 10.1021/jp709896w.

(17) Furman, D.; Wales, D. J. A well-behaved theoretical framework for ReaxFF reactive force fields. *J. Chem. Phys.* **2020**, *153* (2), 021102. DOI: 10.1063/5.0013906.

(18) Mortier, W. J.; Ghosh, S. K.; Shankar, S. Electronegativity-equalization method for the calculation of atomic charges in molecules. *J. Am. Chem. Soc.* **2002**, *108* (15), 4315-4320. DOI: 10.1021/ja00275a013.

(19) van Duin, A. C. T.; Dasgupta, S.; Lorant, F.; Goddard, W. A. ReaxFF: A Reactive Force Field for Hydrocarbons. *J. Phys. Chem. A* **2001**, *105* (41), 9396-9409. DOI: 10.1021/jp004368u.

(20) Hong, S.; van Duin, A. C. T. Atomistic-Scale Analysis of Carbon Coating and Its Effect on the Oxidation of Aluminum Nanoparticles by ReaxFF-Molecular Dynamics Simulations. *J. Phys. Chem. C* **2016**, *120* (17), 9464-9474. DOI: 10.1021/acs.jpcc.6b00786.

(21) Zheng, Y.; Hong, S.; Psofogiannakis, G.; Rayner, G. B., Jr.; Datta, S.; van Duin, A. C. T.; Engel-Herbert, R. Modeling and in Situ Probing of Surface Reactions in Atomic Layer Deposition. *ACS Appl. Mater. Interfaces* **2017**, *9* (18), 15848-15856. DOI: 10.1021/acsami.7b01618.

(22) Jain, A.; Ong, S. P.; Hautier, G.; Chen, W.; Richards, W. D.; Dacek, S.; Cholia, S.; Gunter, D.; Skinner, D.; Ceder, G.; et al. Commentary: The Materials Project: A materials genome approach to accelerating materials innovation. *APL Mater.* **2013**, *1* (1). DOI: 10.1063/1.4812323.

(23) Stukowski, A. Visualization and analysis of atomistic simulation data with OVITO–the Open Visualization Tool. *Model. Simul. Mat. Sci. Eng.* **2010**, *18* (1). DOI: 10.1088/0965-0393/18/1/015012.

(24) Thompson, A. P.; Aktulga, H. M.; Berger, R.; Bolintineanu, D. S.; Brown, W. M.; Crozier, P. S.; in 't Veld, P. J.; Kohlmeyer, A.; Moore, S. G.; Nguyen, T. D.; et al. LAMMPS - a flexible simulation tool for particle-based materials modeling at the atomic, meso, and continuum scales. *Comput. Phys. Commun.* **2022**, *271*. DOI: 10.1016/j.cpc.2021.108171.

(25) Lyakhov, A. O.; Oganov, A. R.; Stokes, H. T.; Zhu, Q. New developments in evolutionary structure prediction algorithm USPEX. *Comput. Phys. Commun.* **2013**, *184* (4), 1172-1182. DOI: 10.1016/j.cpc.2012.12.009.

(26) Martinez, L.; Andrade, R.; Birgin, E. G.; Martinez, J. M. PACKMOL: a package for building initial configurations for molecular dynamics simulations. *J. Comput. Chem.* **2009**, *30* (13), 2157-2164. DOI: 10.1002/jcc.21224.

(27) Kresse, G.; Furthmuller, J. Efficient iterative schemes for ab initio total-energy calculations using a plane-wave basis set. *Phys. Rev. B Condens. Matter* **1996**, *54* (16), 11169-11186. DOI: 10.1103/physrevb.54.11169.

(28) Perdew, J. P.; Burke, K.; Ernzerhof, M. Generalized Gradient Approximation Made Simple. *Phys. Rev. Lett.* **1996**, *77* (18), 3865-3868. DOI: 10.1103/PhysRevLett.77.3865.

(29) Kresse, G.; Joubert, D. From ultrasoft pseudopotentials to the projector augmented-wave method. *Phys. Rev. B* **1999**, *59* (3), 1758-1775. DOI: 10.1103/PhysRevB.59.1758.

(30) Monkhorst, H. J.; Pack, J. D. Special points for Brillouin-zone integrations. *Phys. Rev. B* **1976**, *13* (12), 5188-5192. DOI: 10.1103/PhysRevB.13.5188.

(31) Bedolla, P. O.; Feldbauer, G.; Wolloch, M.; Eder, S. J.; Dorr, N.; Mohn, P.; Redinger, J.; Vernes, A. Effects of van der Waals Interactions in the Adsorption of Isooctane and Ethanol on Fe(100) Surfaces. *J. Phys. Chem. C Nanomater. Interfaces* **2014**, *118* (31), 17608-17615. DOI: 10.1021/jp503829c.

(32) Dion, M.; Rydberg, H.; Schroder, E.; Langreth, D. C.; Lundqvist, B. I. van der Waals density functional for general geometries. *Phys. Rev. Lett.* **2004**, *92* (24), 246401. DOI: 10.1103/PhysRevLett.92.246401.

(33) Roman-Perez, G.; Soler, J. M. Efficient implementation of a van der Waals density functional: application to double-wall carbon nanotubes. *Phys. Rev. Lett.* **2009**, *103* (9), 096102. DOI: 10.1103/PhysRevLett.103.096102.

(34) Klimes, J.; Bowler, D. R.; Michaelides, A. Chemical accuracy for the van der Waals density functional. *J. Phys. Condens. Matter* **2010**, *22* (2), 022201. DOI: 10.1088/0953-8984/22/2/022201.

(35) Nakashima, P. N. H. The Crystallography of Aluminum and Its Alloys. In *Encyclopedia of Aluminum and Its Alloys*, 2019.

(36) LaCount, M. D.; Gygi, F. Ensemble first-principles molecular dynamics simulations of water using the SCAN meta-GGA density functional. *J. Chem. Phys.* **2019**, *151* (16), 164101. DOI: 10.1063/1.5124957.

(37) Sun, C. Q. Scaling relation for the bond length, mass density, and packing order of water ice. *Chem. Phys.* **2013**.

(38) Preobrajenski, A. B.; Lyalin, A.; Taketsugu, T.; Vinogradov, N. A.; Vinogradov, A. S. Honeycomb Boron on Al(111): From the Concept of Borophene to the Two-Dimensional Boride. *ACS Nano.* **2021**, *15* (9), 15153-15165. DOI: 10.1021/acsnano.1c05603.

(39) Berthomieu, D.; Bacquet, Y.; Pedocchi, L.; Goursot, A. Trimethylaluminum Dimer Structure and Its Monomer Radical Cation: A Density Functional Study. *J. Phys. Chem. A* **1998**, *102* (40), 7821-7827. DOI: 10.1021/jp980148t.

(40) Almenningen, A.; Halvorsen, S.; Haaland, A.; Pihlaja, K.; Schaumburg, K.; Ehrenberg, L. A Gas Phase Electron Diffraction Investigation of the Molecular Structures of Trimethylaluminium Monomer and Dimer. *Acta Chem. Scand.* **1971**, *25*, 1937-1945. DOI: 10.3891/acta.chem.scand.25-1937.

Appendix A: Table of ReaxFF Parameters

	Description
pbo1	sigma bond order 1
pbo2	sigma bond order 2
pbo3	pi bond order 1
pbo4	pi bond order 2
pbo5	double pi bond order 1
pbo6	double pi bond order 2
$\lambda 1$	overcoord 1
$\lambda 2$	overcoord 2
$\lambda 3$	bond order correction 1
$\lambda 4$	bond order correction 2
$\lambda 5$	bond order correction 3
$\lambda 6$	bond energy 1
$\lambda 7$	bond energy 2
$\lambda 8$	lone pair valency angle
$\lambda 9$	lone pair energy
$\lambda 10$	overcoordination 1
$\lambda 11$	overcoordination 2
$\lambda 12$	overcoordination penalty
$\lambda 13$	valence angle parameter

λ14	Undercoordination energy 1
λ15	Undercoordination 1
λ16	undercoordination 2
λ17	undercoordination 3
λ18	valence angle 1
λ19	valence angle 2
λ20	valence angle 3
λ21	valence angle 4
λ22	valence angle
λ23	valency undercoordination
λ24	Undercoordination 4
λ25	valency/lone pair
λ26	valency angle 1
λ27	valency angle 2
λ28	penalty energy
λ29	double bond
λ30	double bond overcoord 1
λ31	double bond overcoord 2
λ32	valence conjugation
λ33	valency angle conjugation 1
λ34	valency angle conjugation 2
λ35	valency angle conjugation 3
λ36	torsion angle

$\lambda 37$	torsion bond order
$\lambda 38$	torsion overcoord 1
$\lambda 39$	torsion overcoord 2
$\lambda 40$	torsion conjugation energy
$\lambda 41$	torsion conjugation
$\lambda 42$	hydrogen bond energy
$\lambda 43$	hydrogen bond order
$\lambda 44$	hydrogen bond
$D_e{}^{\sigma}$	sigma dissociation
$D_e{}^{\pi}$	pi dissociation
$D_e{}^{\pi\pi}$	double pi dissociation

Appendix B-1

Reactive MD-force field: Al/C/H/O JPCC, S. Hong and A.C.T. van Duin, J. Phys. Chem. C, 2016, 120 (17), pp 9464-9474, http://dx.doi.org/10.1021/acs.jpcc.6b00786
 39   ! Number of general parameters
   50.0000 !Overcoordination parameter
    9.5469 !Overcoordination parameter
   26.5405 !Valency angle conjugation parameter
    1.7224 !Triple bond stabilisation parameter
    6.8702 !Triple bond stabilisation parameter
   60.4850 !C2-correction
    1.0588 !Undercoordination parameter
    4.6000 !Triple bond stabilisation parameter
   12.1176 !Undercoordination parameter
   13.3056 !Undercoordination parameter
  -70.5044 !Triple bond stabilization energy
    0.0000 !Lower Taper-radius
   10.0000 !Upper Taper-radius
    2.8793 !Not used
   24.5000 !Valency undercoordination
    6.0891 !Valency angle/lone pair parameter
    1.0563 !Valency angle
    2.0384 !Valency angle parameter
    6.1431 !Not used
    6.9290 !Double bond/angle parameter
    0.3989 !Double bond/angle parameter: overcoord
    3.9954 !Double bond/angle parameter: overcoord
   -2.4837 !Not used
    5.7796 !Torsion/BO parameter
   10.0000 !Torsion overcoordination
    1.9487 !Torsion overcoordination
   -1.2327 !Conjugation 0 (not used)
    2.1645 !Conjugation
    1.5591 !vdWaals shielding
    0.1000 !Cutoff for bond order (*100)
    2.1365 !Valency angle conjugation parameter
    0.6991 !Overcoordination parameter
   50.0000 !Overcoordination parameter
    1.8512 !Valency/lone pair parameter
    0.5000 !Not used
   20.0000 !Not used
    5.0000 !Molecular energy (not used)
    0.0000 !Molecular energy (not used)
    2.6962 !Valency angle conjugation parameter
  5   ! Nr of atoms; cov.r; valency;a.m;Rvdw;Evdw;gammaEEM;cov.r2;#
        alfa;gammavdW;valency;Eunder;Eover;chiEEM;etaEEM;n.u.

```
        cov r3;Elp;Heat inc.;n.u.;n.u.;n.u.;n.u.
        ov/un;val1;n.u.;val3,vval4
C   1.3817  4.0000  12.0000  1.8903  0.1838  0.9000  1.1341  4.0000
    9.7559  2.1346  4.0000 34.9350 79.5548  5.9666  7.0000  0.0000
    1.2114  0.0000 202.5551  8.9539 34.9289 13.5366  0.8563  0.0000
   -2.8983  2.5000  1.0564  4.0000  2.9663  0.0000  0.0000  0.0000
H   0.8930  1.0000  1.0080  1.3550  0.0930  0.8203 -0.1000  1.0000
    8.2230 33.2894  1.0000  0.0000 121.1250  3.7248  9.6093  1.0000
   -0.1000  0.0000 61.6606  3.0408  2.4197  0.0003  1.0698  0.0000
  -19.4571  4.2733  1.0338  1.0000  2.8793  0.0000  0.0000  0.0000
O   1.2450  2.0000  15.9990  2.3890  0.1000  1.0898  1.0548  6.0000
    9.7300 13.8449  4.0000 37.5000 116.0768  8.5000  8.3122  2.0000
    0.9049  0.4056 59.0626  3.5027  0.7640  0.0021  0.9745  0.0000
   -3.5500  2.9000  1.0493  4.0000  2.9225  0.0000  0.0000  0.0000
Al  2.4443  3.0000  26.9820  2.0089  0.2161  0.5675 -1.6836  3.0000
   11.8538 16.3962  3.0000  0.0076 16.5151 -0.2451  6.3319  0.0000
   -1.0000  0.0000 67.5458 137.9671  0.2042  0.0000  0.8563  0.0000
  -14.9162  3.0000  1.0338  3.0000  2.5791  0.0000  0.0000  0.0000
X  -0.1000  2.0000  1.0080  2.0000  0.0000  0.0100 -0.1000  6.0000
   10.0000  2.5000  4.0000  0.0000  0.0000  5.000 9999.9999  0.0000
   -0.1000  0.0000 -2.3700  8.7410 13.3640  0.6690  0.9745  0.0000
  -11.0000  2.7466  1.0338  2.0000  2.8793  0.0000  0.0000  0.000
10    ! Nr of bonds; Edis1;LPpen;n.u.;pbe1;pbo5;13corr;pbo6
              pbe2;pbo3;pbo4;n.u.;pbo1;pbo2;ovcorr
1  1 158.2004  99.1897  78.0000 -0.7738 -0.4550  1.0000 37.6117  0.4147
      0.4590 -0.1000  9.1628  1.0000 -0.0777  6.7268  1.0000  0.0000
1  2 169.4760  0.0000  0.0000 -0.6083  0.0000  1.0000  6.0000  0.7652
      5.2290  1.0000  0.0000  1.0000 -0.0500  6.9136  0.0000  0.0000
2  2 153.3934  0.0000  0.0000 -0.4600  0.0000  1.0000  6.0000  0.7300
      6.2500  1.0000  0.0000  1.0000 -0.0790  6.0552  0.0000  0.0000
1  3 158.6946 107.4583  23.3136 -0.4240 -0.1743  1.0000 10.8209  1.0000
      0.5322 -0.3113  7.0000  1.0000 -0.1447  5.2450  0.0000  0.0000
2  3 160.0000  0.0000  0.0000 -0.5725  0.0000  1.0000  6.0000  0.5626
      1.1150  1.0000  0.0000  0.0000 -0.0920  4.2790  0.0000  0.0000
3  3 142.2858 145.0000  50.8293  0.2506 -0.1000  1.0000 29.7503  0.6051
      0.3451 -0.1055  9.0000  1.0000 -0.1225  5.5000  1.0000  0.0000
1  4 106.1950  0.0000  0.0000  0.6481 -0.3000  0.0000 36.0000  0.0100
      3.5736 -0.3500  25.0000  1.0000 -0.1947  4.8726  0.0000  0.0000
2  4  78.5674  0.0000  0.0000 -0.5170 -0.3000  0.0000 36.0000  0.0100
     13.0000 -0.3500  25.0000  1.0000 -0.1044  5.6108  0.0000  0.0000
3  4 175.2517  0.0000  0.0000 -0.8707 -0.3000  0.0000 36.0000  0.0100
      0.9278 -0.3500  25.0000  1.0000 -0.1183  4.6533  0.0000  0.0000
4  4  65.7742  0.0000  0.0000 -0.4111 -0.3000  0.0000 16.0000  0.2955
      2.8637 -0.4197  14.3085  1.0000 -0.1993  4.8757  0.0000  0.0000
6    ! Nr of off-diagonal terms; Ediss;Ro;gamma;rsigma;rpi;rpi2
1  2  0.1239  1.4004  9.8467  1.1210 -1.0000 -1.0000
```

```
1 3   0.1156   1.8520   9.8317   1.2854   1.1352   1.0706
2 3   0.0283   1.2885   10.9190   0.9215   -1.0000   -1.0000
1 4   0.3468   1.4082   12.8976   1.5543   -1.0000   -1.0000
2 4   0.0549   1.3617   12.7585   1.7073   -1.0000   -1.0000
3 4   0.3745   1.8179   9.7359   1.4165   -1.0000   -1.0000
37   ! Nr of angles;at1;at2;at3;Thetao,o;ka;kb;pv1;pv2
1 1 1   59.0573   30.7029   0.7606   0.0000   0.7180   6.2933   1.1244
1 1 2   65.7758   14.5234   6.2481   0.0000   0.5665   0.0000   1.6255
2 1 2   70.2607   25.2202   3.7312   0.0000   0.0050   0.0000   2.7500
1 1 3   49.6811   7.1713   4.3889   0.0000   0.7171   10.2661   1.0463
2 1 3   65.0000   13.8815   5.0583   0.0000   0.4985   0.0000   1.4900
3 1 3   77.7473   40.1718   2.9802   -25.3063   1.6170   -46.1315   2.2503
1 2 1   0.0000   3.4110   7.7350   0.0000   0.0000   0.0000   1.0400
1 2 2   0.0000   0.0000   6.0000   0.0000   0.0000   0.0000   1.0400
1 2 3   0.0000   25.0000   3.0000   0.0000   1.0000   0.0000   1.0400
2 2 2   0.0000   27.9213   5.8635   0.0000   0.0000   0.0000   1.0400
2 2 3   0.0000   8.5744   3.0000   0.0000   0.0000   0.0000   1.0421
3 2 3   0.0000   15.0000   2.8900   0.0000   0.0000   0.0000   2.8774
1 3 1   73.5312   44.7275   0.7354   0.0000   3.0000   0.0000   1.0684
1 3 3   79.4761   36.3701   1.8943   0.0000   0.7351   67.6777   3.0000
1 3 2   70.1880   20.9562   0.3864   0.0000   0.0050   0.0000   1.6924
2 3 2   85.8000   9.8453   2.2720   0.0000   2.8635   0.0000   1.5800
2 3 3   75.6935   50.0000   2.0000   0.0000   1.0000   0.0000   1.1680
3 3 3   80.7324   30.4554   0.9953   0.0000   1.6310   50.0000   1.0783
1 3 4   90.0000   5.0000   3.0000   0.0000   1.0000   0.0000   1.1000
2 3 4   90.0000   11.1212   4.3379   0.0000   3.0000   0.0000   3.0000
3 3 4   43.6280   11.0750   6.6200   0.0000   3.0000   0.0000   1.0100
4 3 4   64.5513   10.5987   1.0471   0.0000   3.0000   0.0000   1.6045
3 4 3   84.7469   7.3926   2.9453   0.0000   0.1000   0.0000   1.2535
3 4 4   27.4957   14.3276   0.2771   0.0000   2.3158   0.0000   2.2134
1 4 1   71.5643   40.0000   0.7916   0.0000   0.0230   0.0000   1.0011
4 1 4   1.0000   39.3256   10.0000   0.0000   0.4988   0.0000   1.3731
2 1 4   77.3364   13.9658   9.8503   0.0000   0.1352   0.0000   1.0000
1 4 3   74.5260   40.0000   2.4295   0.0000   1.8739   0.0000   1.0010
1 1 4   26.5597   9.1438   8.4576   0.0000   2.3277   0.0000   1.4756
1 4 4   39.5036   6.3913   0.9117   0.0000   2.6905   0.0000   3.0000
2 4 2   100.0000   5.9042   0.0871   0.0000   3.0000   0.0000   1.0100
2 4 4   10.0000   4.2493   0.4967   0.0000   0.1000   0.0000   1.9554
2 4 4   180.0000   -22.9923   5.1657   0.0000   0.8783   0.0000   2.3156
4 2 4   0.0000   10.9458   0.1218   0.0000   0.1000   0.0000   1.0588
2 2 4   0.0000   2.0796   1.0424   0.0000   1.5070   0.0000   1.2393
1 4 2   79.1340   0.2838   3.8832   0.0000   0.1001   0.0000   3.0000
1 2 4   0.0000   0.0100   0.0100   0.0000   0.7901   0.0000   2.9774
26   ! Nr of torsions;at1;at2;at3;at4;;V1;V2;V3;V2(BO);vconj;n.u;n
1 1 1 1   -0.2500   34.7453   0.0288   -6.3507   -1.6000   0.0000   0.0000
1 1 1 2   -0.2500   29.2131   0.2945   -4.9581   -2.1802   0.0000   0.0000
```

```
2 1 1 2 -0.2500 31.2081  0.4539 -4.8923 -2.2677  0.0000  0.0000
1 1 1 3 -0.3495 22.2142 -0.2959 -2.5000 -1.9066  0.0000  0.0000
2 1 1 3  0.0646 24.3195  0.6259 -3.9603 -1.0000  0.0000  0.0000
3 1 1 3 -0.5456  5.5756  0.8433 -5.1924 -1.0180  0.0000  0.0000
1 1 3 1  1.7555 27.9267  0.0072 -2.6533 -1.0000  0.0000  0.0000
1 1 3 2 -1.4358 36.7830 -1.0000 -8.1821 -1.0000  0.0000  0.0000
2 1 3 1 -1.3959 34.5053  0.7200 -2.5714 -2.1641  0.0000  0.0000
2 1 3 2 -2.5000 70.0597  1.0000 -3.5539 -2.9929  0.0000  0.0000
1 1 3 3  0.6852 11.2819 -0.4784 -2.5000 -2.1085  0.0000  0.0000
2 1 3 3  0.1933 80.0000  1.0000 -4.0590 -3.0000  0.0000  0.0000
3 1 3 1 -1.9889 76.4820 -0.1796 -3.8301 -3.0000  0.0000  0.0000
3 1 3 2  0.2160 72.7707 -0.7087 -4.2100 -3.0000  0.0000  0.0000
3 1 3 3 -2.5000 71.0772  0.2542 -3.1631 -3.0000  0.0000  0.0000
1 3 3 1  2.5000 -0.6002  1.0000 -3.4297 -2.8858  0.0000  0.0000
1 3 3 2 -2.5000 -3.3822  0.7004 -5.4467 -2.9586  0.0000  0.0000
2 3 3 2  2.5000 -4.0000  0.9000 -2.5000 -1.0000  0.0000  0.0000
1 3 3 3  1.2329 -4.0000  1.0000 -2.5000 -1.7479  0.0000  0.0000
2 3 3 3  0.8302 -4.0000 -0.7763 -2.5000 -1.0000  0.0000  0.0000
3 3 3 3 -2.5000 -4.0000  1.0000 -2.5000 -1.0000  0.0000  0.0000
0 1 2 0  0.0000  0.0000  0.0000  0.0000  0.0000  0.0000  0.0000
0 2 2 0  0.0000  0.0000  0.0000  0.0000  0.0000  0.0000  0.0000
0 2 3 0  0.0000  0.1000  0.0200 -2.5415  0.0000  0.0000  0.0000
0 1 1 0  0.0000 50.0000  0.3000 -4.0000 -2.0000  0.0000  0.0000
0 3 3 0  0.5511 25.4150  1.1330 -5.1903 -1.0000  0.0000  0.0000
1    ! Nr of hydrogen bonds;at1;at2;at3;Rhb;Dehb;vhb1
3 2 3  2.1200 -3.5800  1.4500 19.5000
```

Appendix B-2

Reactive MD-force field: TMA/Ge/C/H/O
 39   ! Number of general parameters
   50.0000 !p_boc1 Eq(4c): Overcoordination parameter
    9.5469 !p_boc2 Eq(4d): Overcoordination parameter
   26.5405 !p_coa2 Eq(15): Valency angle conjugation
    1.7224 !p_trip4 Eq(20): Triple bond stabilisation
    6.8702 !p_trip3 Eq(20): Triple bond stabilisation
   60.4850 !k_c2 Eq(19): C2-correction
    1.0588 !p_ovun6 Eq(12): Undercoordination
    4.6000 !p_trip2 Eq(20): Triple bond stabilisation
   12.1176 !p_ovun7 Eq(12): Undercoordination
   13.3056 !p_ovun8 Eq(12): Undercoordination
  -70.5044 !p_trip1 Eq(20): Triple bond stabilization
    0.0000 !Lower Taper-radius (must be 0)
   10.0000 !R_cut Eq(21): Upper Taper-radius
    2.8793 !p_fe1 Eq(6a): Fe dimer correction
   33.8667 !p_val6 Eq(13c): Valency undercoordination
    6.0891 !p_lp1 Eq(8): Lone pair param
    1.0563 !p_val9 Eq(13f): Valency angle exponent
    2.0384 !p_val10 Eq(13g): Valency angle parameter
    6.1431 !p_fe2 Eq(6a): Fe dimer correction
    6.9290 !p_pen2 Eq(14a): Double bond/angle param
    0.3989 !p_pen3 Eq(14a): Double bond/angle param
    3.9954 !p_pen4 Eq(14a): Double bond/angle param
   -2.4837 !p_fe3 Eq(6a): Fe dimer correction
    5.7796 !p_tor2 Eq(16b): Torsion/BO parameter
   10.0000 !p_tor3 Eq(16c): Torsion overcoordination
    1.9487 !p_tor4 Eq(16c): Torsion overcoordination
   -1.2327 !p_elho Eq(26a): electron-hole interaction
    2.1645 !p_cot2 Eq(17b): Conjugation if tors13=0
    1.5591 !p_vdW1 Eq(23b): vdWaals shielding
    0.1000 !Cutoff for bond order (*100)
    2.1365 !p_coa4 Eq(15): Valency angle conjugation
    0.6991 !p_ovun4 Eq(11b): Over/Undercoordination
   50.0000 !p_ovun3 Eq(11b): Over/Undercoordination
    1.8512 !p_val8 Eq(13d): Valency/lone pair param
    0.5000 !X_soft Eq(25): ACKS2 softness for X_ij
   20.0000 !d Eq(23d): Scale factor in lg-dispersion
    5.0000 !p_val Eq(27): Gauss exponent for electrons
    0.0000 !1 Eq(13e): disable undecoord in val angle
    2.6962 !p_coa3 Eq(15): Valency angle conjugation
  6   ! Nr of atoms; cov.r; valency;a.m;Rvdw;Evdw;gammaEEM;cov.r2;#
         alfa;gammavdW;valency;Eunder;Eover;chiEEM;etaEEM;n.u.
         cov r3;Elp;Heat inc.;bo131;bo132;bo133;softcut;n.u.

ov/un;val1;n.u.;val3,vval4
C   1.3817   4.0000 12.0000   1.8903   0.1838   0.9000   1.1341   4.0000
    9.7559   2.1346   4.0000 34.9350 79.5548   5.9666   7.0000   0.0000
    1.2114   0.0000 202.5551   8.9539 34.9289 13.5366   0.8563   0.0000
   -2.8983   2.5000   1.0564   4.0000   2.9663   0.0000   0.0000   0.0000
H   0.8930   1.0000   1.0080   1.3550   0.0930   0.8203 -0.1000   1.0000
    8.2230 33.2894   1.0000   0.0000 121.1250   3.7248   9.6093   1.0000
   -0.1000   0.0000 61.6606   3.0408   2.4197   0.0003   1.0698   0.0000
  -19.4571   4.2733   1.0338   1.0000   2.8793   0.0000   0.0000   0.0000
O   1.2450   2.0000 15.9990   2.3890   0.1000   1.0898   1.0548   6.0000
    9.7300 13.8449   4.0000 37.5000 116.0768   8.5000   8.3122   2.0000
    0.9049   0.4056 59.0626   3.5027   0.7640   0.0021   0.9745   0.0000
   -3.5500   2.9000   1.0493   4.0000   2.9225   0.0000   0.0000   0.0000
Al 2.4443   3.0000 26.9820   2.0089   0.2161   0.5675 -1.6836   3.0000
   11.8538 16.3962   3.0000   0.0076 16.5151 -0.2451   6.3319   0.0000
   -1.0000   0.0000 67.5458 137.9671   0.2042   0.0000   0.8563   0.0000
  -14.9162   3.0000   1.0338   3.0000   2.5791   0.0000   0.0000   0.0000
Ge 2.0804   4.0000 72.6100   2.5441   0.1939   0.3000   0.9578   4.0000
   11.9727   1.0000   4.0000 10.5217 131.4200   4.2027   6.0120   0.0000
   -1.0000   0.0000 128.9891   8.7895 23.9298   0.8381   0.8563   0.0000
   -4.0000   3.0365   1.0338   6.2998   2.5791   0.0000   0.0000   0.0000
X -0.1000   2.0000   1.0080   2.0000   0.0000   0.0100 -0.1000   6.0000
   10.0000   2.5000   4.0000   0.0000   0.0000   5.0000 9999.9999   0.0000
   -0.1000   0.0000 -2.3700   8.7410 13.3640   0.6690   0.9745   0.0000
  -11.0000   2.7466   1.0338   2.0000   2.8793   0.0000   0.0000   0.0000
15   ! Nr of bonds; Edis1;LPpen;n.u.;pbe1;pbo5;13corr;pbo6
               pbe2;pbo3;pbo4;n.u.;pbo1;pbo2;ovcorr
 1 1 158.2004 99.1897 78.0000 -0.7738 -0.4550   1.0000 37.6117   0.4147
       0.4590 -0.1000   9.1628   1.0000 -0.0777   6.7268   1.0000   0.0000
 1 2 169.4760   0.0000   0.0000 -0.6083   0.0000   1.0000   6.0000   0.7652
       5.2290   1.0000   0.0000   1.0000 -0.0500   6.9136   0.0000   0.0000
 2 2 153.3934   0.0000   0.0000 -0.4600   0.0000   1.0000   6.0000   0.7300
       6.2500   1.0000   0.0000   1.0000 -0.0790   6.0552   0.0000   0.0000
 1 3 158.6946 107.4583 23.3136 -0.4240 -0.1743   1.0000 10.8209   1.0000
       0.5322 -0.3113   7.0000   1.0000 -0.1447   5.2450   0.0000   0.0000
 2 3 160.0000   0.0000   0.0000 -0.5725   0.0000   1.0000   6.0000   0.5626
       1.1150   1.0000   0.0000   0.0000 -0.0920   4.2790   0.0000   0.0000
 3 3 142.2858 145.0000 50.8293   0.2506 -0.1000   1.0000 29.7503   0.6051
       0.3451 -0.1055   9.0000   1.0000 -0.1225   5.5000   1.0000   0.0000
 1 4 124.6651   0.0000   0.0000   0.8374 -0.3000   0.0000 36.0000   0.0100
       1.8311 -0.3500 25.0000   1.0000 -0.2337   4.6603   0.0000   0.0000
 2 4 88.1357   0.0000   0.0000 -0.6715 -0.3000   0.0000 36.0000   0.0208
       9.9192 -0.3500 25.0000   1.0000 -0.1014   5.5268   0.0000   0.0000
 3 4 175.2517   0.0000   0.0000 -0.8707 -0.3000   0.0000 36.0000   0.0100
       0.9278 -0.3500 25.0000   1.0000 -0.1183   4.6533   0.0000   0.0000
 4 4 65.7742   0.0000   0.0000 -0.4111 -0.3000   0.0000 16.0000   0.2955

```
       2.8637  -0.4197  14.3085   1.0000  -0.1993   4.8757   0.0000   0.0000
 5  5  95.1003  63.0193  30.0000   0.1000  -0.3000   1.0000  16.0000   0.0755
       0.1062  -0.6420   6.1811   1.0000  -0.0602   8.1721   0.0000   0.0000
 2  5 197.2565   0.0000   0.0000  -0.4949   0.0000   1.0000   6.0000   0.5000
      14.0700   1.0000   0.0000   1.0000  -0.0822   5.0948   0.0000   0.0000
 3  5 179.4669  27.3037  43.3991  -0.4799  -0.3000   1.0000  36.0000   0.1561
       9.5978  -0.6031   5.8440   1.0000  -0.1590   5.8144   1.0000   0.0000
 1  5 161.4618  47.6708  43.3991  -1.0000  -0.3000   1.0000  36.0000   0.0421
      10.0094  -1.2556  14.0726   1.0000  -0.0661   6.5965   1.0000   0.0000
 4  5 139.6885   0.0000   0.0000  -0.4520  -0.2000   0.0000  16.0000   0.5199
       8.1108  -0.2000  15.0000   1.0000  -0.1108   4.0729   0.0000   0.0000
10   ! Nr of off-diagonal terms; Ediss;Ro;gamma;rsigma;rpi;rpi2
 1  2   0.1239   1.4004   9.8467   1.1210  -1.0000  -1.0000
 1  3   0.1156   1.8520   9.8317   1.2854   1.1352   1.0706
 2  3   0.0283   1.2885  10.9190   0.9215  -1.0000  -1.0000
 1  4   0.3393   1.4683  12.5362   1.4713  -1.0000  -1.0000
 2  4   0.0616   1.4846  11.6504   1.6956  -1.0000  -1.0000
 3  4   0.3745   1.8179   9.7359   1.4165  -1.0000  -1.0000
 2  5   0.0656   1.3939  13.6170   1.2520  -1.0000  -1.0000
 3  5   0.1009   1.7484  12.4527   1.7770   1.3682  -1.0000
 1  5   0.2655   1.9097  11.1886   1.9983   1.3682  -1.0000
 4  5   0.2000   2.1000  11.5000   1.9916  -1.0000  -1.0000
67    ! Nr of angles;at1;at2;at3;Thetao,o;ka;kb;pv1;pv2
 1  1  1  59.0573  30.7029   0.7606   0.0000   0.7180   6.2933   1.1244
 1  1  2  65.7758  14.5234   6.2481   0.0000   0.5665   0.0000   1.6255
 2  1  2  70.2607  25.2202   3.7312   0.0000   0.0050   0.0000   2.7500
 1  1  3  49.6811   7.1713   4.3889   0.0000   0.7171  10.2661   1.0463
 2  1  3  65.0000  13.8815   5.0583   0.0000   0.4985   0.0000   1.4900
 3  1  3  77.7473  40.1718   2.9802 -25.3063   1.6170 -46.1315   2.2503
 1  2  1   0.0000   3.4110   7.7350   0.0000   0.0000   0.0000   1.0400
 1  2  2   0.0000   0.0000   6.0000   0.0000   0.0000   0.0000   1.0400
 1  2  3   0.0000  25.0000   3.0000   0.0000   1.0000   0.0000   1.0400
 2  2  2   0.0000  27.9213   5.8635   0.0000   0.0000   0.0000   1.0400
 2  2  3   0.0000   8.5744   3.0000   0.0000   0.0000   0.0000   1.0421
 3  2  3   0.0000  15.0000   2.8900   0.0000   0.0000   0.0000   2.8774
 1  3  1  73.5312  44.7275   0.7354   0.0000   3.0000   0.0000   1.0684
 1  3  3  79.4761  36.3701   1.8943   0.0000   0.7351  67.6777   3.0000
 1  3  2  70.1880  20.9562   0.3864   0.0000   0.0050   0.0000   1.6924
 2  3  2  85.8000   9.8453   2.2720   0.0000   2.8635   0.0000   1.5800
 2  3  3  75.6935  50.0000   2.0000   0.0000   1.0000   0.0000   1.1680
 3  3  3  80.7324  30.4554   0.9953   0.0000   1.6310  50.0000   1.0783
 1  3  4 104.6094  27.2324   9.0549   0.0000   2.3214   0.0000   1.1378
 2  3  4  90.0000  11.1212   4.3379   0.0000   3.0000   0.0000   3.0000
 3  3  4  43.6280  11.0750   6.6200   0.0000   3.0000   0.0000   1.0100
 4  3  4  64.5513  10.5987   1.0471   0.0000   3.0000   0.0000   1.6045
 3  4  3  84.7469   7.3926   2.9453   0.0000   0.1000   0.0000   1.2535
```

```
3 4 4  27.4957 14.3276  0.2771  0.0000  2.3158  0.0000  2.2134
1 4 1  51.9685 44.5007  3.5568  0.0000  1.5137  0.0000  1.0170
4 1 4   1.0000 32.3336  8.0478  0.0000  0.1476  0.0000  1.0537
2 1 4  80.6030 30.7117  9.8117  0.0000  0.6965  0.0000  2.1354
1 4 3  85.0931 44.6258  2.0213  0.0000  1.7462  0.0000  1.1565
1 1 4  19.4475  2.2656  8.7606  0.0000  2.3143  0.0000  1.6903
1 4 4  39.3013 12.9114  0.5761  0.0000  3.0000  0.0000  2.8613
2 4 2  79.7991  0.1000  0.1000  0.0000  1.4104  0.0000  1.4114
2 4 4   4.0000 25.8806  0.6357  0.0000  0.5039  0.0000  2.3628
2 4 4 180.0000 -40.0000  2.3424  0.0000  1.2344  0.0000  1.0100
4 2 4   0.0000 10.9458  0.1218  0.0000  0.1000  0.0000  1.0588
2 2 4   0.0000  1.4899  1.8813  0.0000  1.5753  0.0000  1.2147
1 4 2  49.9808  4.4654  7.6824  0.0000  0.1213  0.0000  2.8840
1 2 4   0.0000  0.1000  0.1300  0.0000  0.6694  0.0000  2.9331
5 5 5  66.6054 16.3154  1.4405  0.0000  0.0133  0.0000  1.1339
2 2 5   0.0000 65.0379  8.0587  0.0000  1.6371  0.0000  2.1153
2 5 5  73.5323 10.0544 15.3457  0.0000  0.0651  0.0000  1.3384
2 5 2  71.8258 73.4083  8.5880  0.0000  2.8421  0.0000  1.6822
5 2 5   0.0000 69.5047 11.1621  0.0000  1.6371  0.0000  1.7493
3 5 5  89.7858 30.0940  3.0721  0.0000  0.3513  0.0000  2.8039
2 5 3  49.4808 19.2621  2.6641  0.0000  4.0000  0.0000  1.0000
3 5 3  80.7790  6.2479  1.3924  0.0000  3.2162  0.0000  1.0300
5 3 5  23.7087 10.9382  0.9520  0.0000  4.0000  0.0000  1.0000
2 3 5  69.7422 10.3770  9.2233  0.0000  1.1748  0.0000  1.0000
3 3 5  87.5684 18.2823  1.9481  0.0000  1.3815  0.0000  1.0739
1 5 5  55.5918 23.6896  2.1318  0.0000  3.6469  0.0000  1.9055
1 5 2  76.3376 18.8721  4.1229  0.0000  0.9194  0.0000  1.2935
1 5 1 100.0000  6.5114  2.5828  0.0000  0.6427  0.0000  1.5529
5 1 5  44.0075  2.7819  0.6763  0.0000  3.6755  0.0000  1.1903
2 1 5  88.8773 12.8751  9.3121  0.0000  3.0000  0.0000  1.0000
1 1 5  96.2951 18.3964  1.7282  0.0000  2.2703  0.0000  1.1962
4 3 5  18.1470 15.7705  4.8158  0.0000  2.9694  0.0000  2.4579
1 3 5 110.0000 27.5093  5.4413  0.0000  1.7696  0.0000  1.0000
1 5 3  65.7436 35.5076  1.3133  0.0000  0.1000  0.0000  2.9900
3 1 5  65.9044 14.7880  2.1288  0.0000  1.5443  0.0000  1.0000
1 2 5   0.0000  5.4180  1.3319  0.0000  1.3813  0.0000  1.0000
4 5 5  79.0746 31.3352  1.0637  0.0000  0.3650  0.0000  1.7765
2 5 4  79.1629 30.0000  1.3369  0.0000  0.1000  0.0000  2.2224
1 4 5 100.0000 25.4959  2.2946  0.0000  1.3555  0.0000  1.0000
3 4 5 110.0000  5.0000  3.0000  0.0000  0.9666  0.0000  1.5272
3 5 4  51.5018  3.5344  3.0000  0.0000  0.7694  0.0000  1.0000
2 4 5  68.4251 20.2143  2.1352  0.0000  0.5873  0.0000  1.3481
5 4 5  90.6054  5.3154  1.4405  0.0000  0.0133  0.0000  1.1339
4 2 5   0.0000 31.4046  5.8335  0.0000  1.6371  0.0000  1.0400
26    ! Nr of torsions;at1;at2;at3;at4;;V1;V2;V3;V2(BO);vconj;n.u;n
 1 1 1 1  -0.2500 34.7453  0.0288  -6.3507  -1.6000  0.0000  0.0000
```

```
1 1 1 2 -0.2500 29.2131  0.2945 -4.9581 -2.1802  0.0000  0.0000
2 1 1 2 -0.2500 31.2081  0.4539 -4.8923 -2.2677  0.0000  0.0000
1 1 1 3 -0.3495 22.2142 -0.2959 -2.5000 -1.9066  0.0000  0.0000
2 1 1 3  0.0646 24.3195  0.6259 -3.9603 -1.0000  0.0000  0.0000
3 1 1 3 -0.5456  5.5756  0.8433 -5.1924 -1.0180  0.0000  0.0000
1 1 3 1  1.7555 27.9267  0.0072 -2.6533 -1.0000  0.0000  0.0000
1 1 3 2 -1.4358 36.7830 -1.0000 -8.1821 -1.0000  0.0000  0.0000
2 1 3 1 -1.3959 34.5053  0.7200 -2.5714 -2.1641  0.0000  0.0000
2 1 3 2 -2.5000 70.0597  1.0000 -3.5539 -2.9929  0.0000  0.0000
2 1 3 3  0.1933 80.0000  1.0000 -4.0590 -3.0000  0.0000  0.0000
3 1 3 1 -1.9889 76.4820 -0.1796 -3.8301 -3.0000  0.0000  0.0000
3 1 3 2  0.2160 72.7707 -0.7087 -4.2100 -3.0000  0.0000  0.0000
1 3 3 2 -2.5000 -3.3822  0.7004 -5.4467 -2.9586  0.0000  0.0000
2 3 3 2  2.5000 -4.0000  0.9000 -2.5000 -1.0000  0.0000  0.0000
1 3 3 3  1.2329 -4.0000  1.0000 -2.5000 -1.7479  0.0000  0.0000
2 3 3 3  0.8302 -4.0000 -0.7763 -2.5000 -1.0000  0.0000  0.0000
3 3 3 3 -2.5000 -4.0000  1.0000 -2.5000 -1.0000  0.0000  0.0000
0 1 2 0  0.0000  0.0000  0.0000  0.0000  0.0000  0.0000  0.0000
0 2 2 0  0.0000  0.0000  0.0000  0.0000  0.0000  0.0000  0.0000
0 2 3 0  0.0000  0.1000  0.0200 -2.5415  0.0000  0.0000  0.0000
0 1 1 0  0.0000 50.0000  0.3000 -4.0000 -2.0000  0.0000  0.0000
0 3 3 0  0.5511 25.4150  1.1330 -5.1903 -1.0000  0.0000  0.0000
1 1 3 3 -2.0000 73.0530  1.5000 -9.0000 -2.0000  0.0000  0.0000
1 3 3 1  0.0002 80.0000 -1.5000 -2.5000 -2.0000  0.0000  0.0000
3 1 3 3 -1.8835 20.0000  1.5000 -9.0000 -2.0000  0.0000  0.0000
1    ! Nr of hydrogen bonds;at1;at2;at3;Rhb;Dehb;vhb1
3 2 3  2.1200 -3.5800  1.4500 19.5000
```